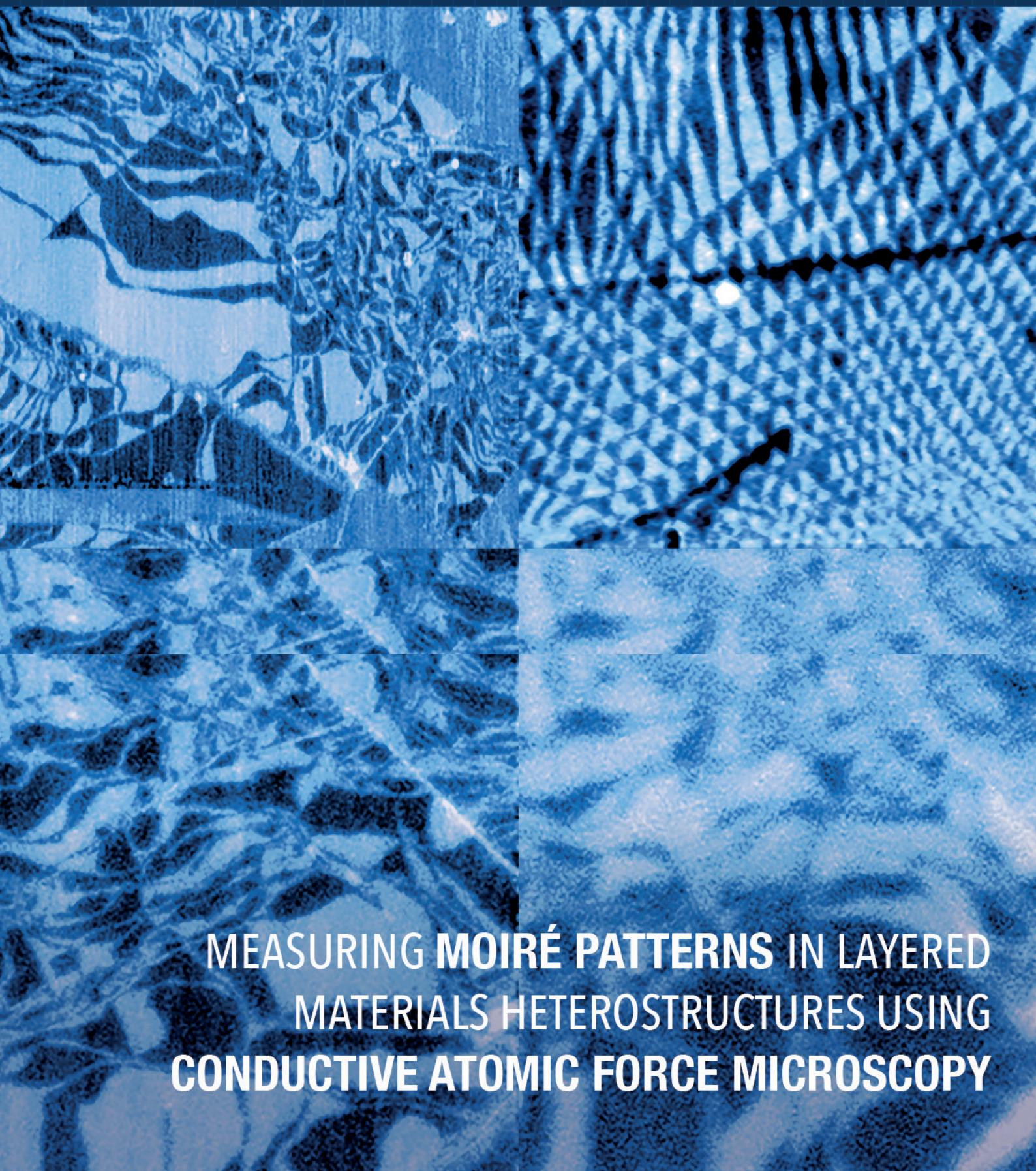


The Magazine for Nano Science and Technology

VOL 24 SPRING 2023

NANOscientific



**MEASURING MOIRÉ PATTERNS IN LAYERED
MATERIALS HETEROSTRUCTURES USING
CONDUCTIVE ATOMIC FORCE MICROSCOPY**

Welcome from the Editor

NanoScientific Interview

Dr. Kim Mckelvey, Victoria University of Wellington, New Zealand

Characterization of 2D materials by imaging spectroscopic ellipsometry (ISE)

Peter H. Thiesen, Application Specialist, Park Systems GmbH

Functional polymeric passivation-led improvement of bias stress with long-term durability of edge-rich nanoporous MoS₂ thin-film transistors

Heekyeong Park (Harvard University, USA), Junhwan Choi (KAIST, Republic of Korea), Junoh Shim (SKKU, Republic of Korea), Seung Min Lee (KAIST, Republic of Korea), Sungmin On (Pohang Accelerator Laboratory, Republic of Korea) et al

How to tailor the crystallographic orientation evolution and surface morphological features of polycrystalline conductive N-type ZnO films

Tetsuya Yamamoto, Research Institute, Kochi University of Technology, Japan

NanoScientific Interview

Pioneering Film Deposition Technology Unconstrained By The Field Framework

Prof. Tetsuya Yamamoto, Research Institute, Kochi University of Technology, Japan

Surface potential characterization of two-dimensional materials through back-gate voltage biases

Seok-Ju Kang, Jong Yun Kim, Oh Hun Gwon, and Young-Jun Yu. Department of Physics, Chungnam National University, Korea. Jaekyung Kim, Park Systems Corp., Suwon, Korea

Mapping the registry and functional properties of layered materials heterostructures using conductive atomic force microscopy

J. Kerfoot, V. V. Korolkov. Park Systems UK Ltd, Nottingham, UK

Park Systems News

Park Systems introduces Park NX-IR R300 and Park NanoStandard
Park Systems Corporation acquires Accurion GmbH

3

4

6

9

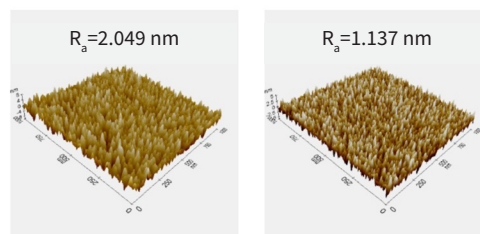
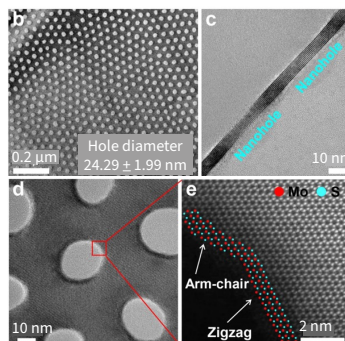
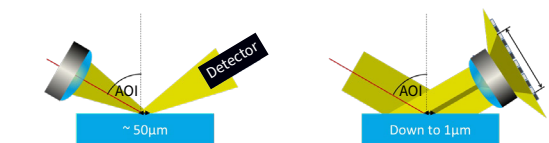
13

16

18

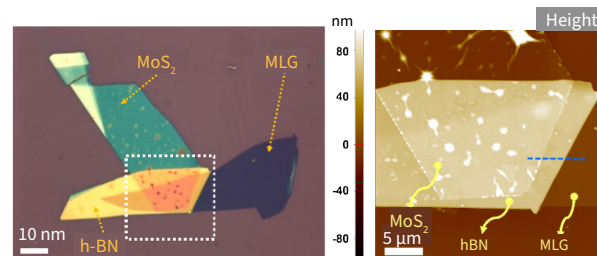
21

25



dc-MS-AZO

rf-MS-AZO



- **Keibock Lee**, Editor-in-Chief
keibock@nanoscientific.org
- **Jessica Kang**, Managing Editor
- **Johnny Kim**, Editor and Point of Contact
johnny@nanoscientific.org
- **Cherie Jung**, Marketing Manager
- **Ester Cho**, Art Director

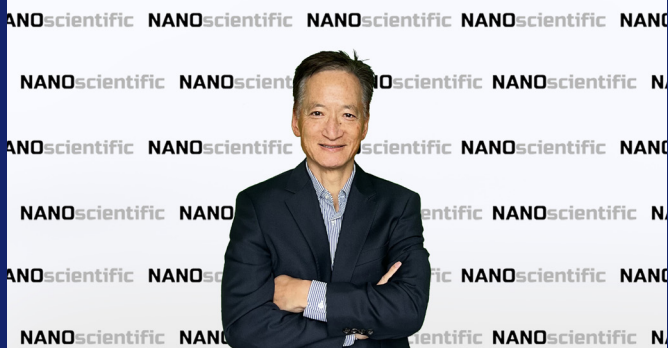
- Publisher and Corporate officers**
- **Sang-il Park**, Chief Executive Officer
 - **Sang-Joon Cho**: EVP of Sales
 - **Richard Lee**: EVP of Product Marketing

NanoScientific is published both in print and online to showcase advancements in the field of nanoscience and technology across a wide range of multidisciplinary

areas of research. The publication is offered free to anyone who works or have interest in the field of nanotechnology, nanoscience, microscopy and other related fields of study and manufacturing.

We enjoy hearing from you, our readers. Please send your research or story ideas to johnny@nanoscientific.org.

To view all of our articles, please visit our web site at magazine.nanoscientific.org.



MESSAGE FROM EDITOR

Welcome to the 24th edition of NanoScientific. We are thrilled to announce that the NanoScientific magazine, both in print and online, is resuming its publication based on the overwhelming interest from our past avid readers.

In this edition, we delve into the fascinating world of 2D materials research and the nanoscale microscopy tools that are being used to study them. 2D materials have been a subject of research interest for many years, but recent advances in technology have led to a surge in research activities focused on these materials. Graphene, the most famous 2D material, has exceptional thermal and electrical conductivity properties, making it a promising material for a wide range of applications such as electronics, energy storage, and biomedicine. However, there are many other 2D materials with unique properties and potential applications.

The challenge with studying 2D materials is their small size, which makes them difficult to observe and manipulate using conventional microscopy techniques. This is where nanoscale microscopy tools come in. Atomic force microscopy (AFM) and imaging spectroscopic ellipsometry (ISE) are powerful tools that can be used to image and characterize 2D materials at the atomic and optical level, respectively. However, more specialized tools like scanning electrochemical cell microscopy (SECCM) and conductive atomic force microscopy (C-AFM) are used to further advance the field of 2D materials research.

The future of 2D materials research looks bright, and the development of new nanoscale techniques using the AFM, ISE, SECCM and C-AFM will drive further advancements in the field. In this edition of NanoScientific, we present the latest research on 2D materials, and the microscopy methods used to study them. We hope that this issue will serve as an essential resource for researchers and enthusiasts alike, and we look forward to keeping you updated with the latest developments in nanoscience and technology.

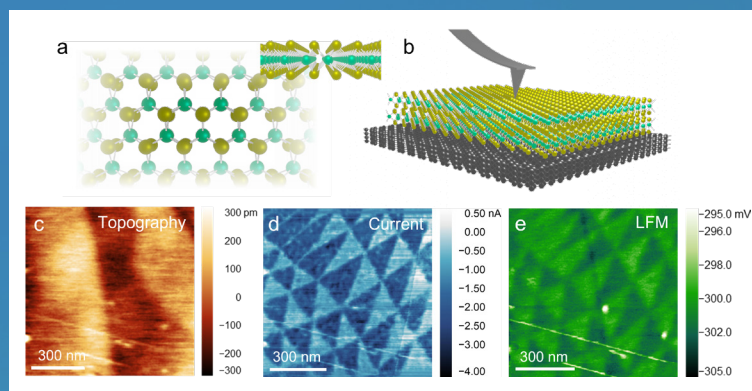
Last but not least, NanoScientific Symposiums are back this year, following a successful run of virtual and live events during these past years—the symposium that brought together thousands of people from nearly 40 countries and awarded cash prizes for presenters and poster exhibits. Abstracts are now being accepted for this year's symposiums, with the chance to be a presenter and win cash prizes. Park Systems is the main supporter of NanoScientific, adhering to its mission of enabling scientific advances.

Keibock Lee
Chief Editor

magazine.nanoscientific.org

MAPPING PROPERTIES OF LAYERED MATERIALS HETEROSTRUCTURES WITH CONDUCTIVE AFM

This article discusses the use of conductive atomic force microscopy (C-AFM) in determining the registry of layers and extracting functional properties of layered materials heterostructures via spectroscopic measurements over individual features. Manipulating the registry of layers within layered materials heterostructures leads to changes in their functional properties, both locally and at scales relevant to devices. Conductive AFM utilizes the same setup as contact mode AFM to maintain the tip in contact with the surface under constant mechanical load via a feedback loop which also allows the topography to be extracted.



By applying an electrical contact to the sample and using a conductive probe, the current may be measured at the tip-sample junction and mapped spatially with sub-nanometer resolution. The article also highlights the phenomenon of moiré patterns, which occur when two rigid layers with a fixed spatial periodicity are overlaid. Moiré patterns can be observed in many situations including in overlaid fabrics, bridges, and most recently, in layered materials heterostructures. When using C-AFM, structures are immediately observed in the current channel without significant modification of setpoints. The study was conducted using Park FX40 AFM (www.parksystems.com/fx40). Read the complete article on page 22.

NANOSCIENTIFIC INTERVIEW

WITH DR. KIM MCKELVEY

This interview is a follow up to Dr. McKelvey's recent article published In Nature journal: Isolation of pseudocapacitive surface processes at monolayer MXene flakes reveals delocalized charging mechanism. <https://doi.org/10.1038/s41467-023-35950-1>

About Dr. Kim McKelvey

Dr. McKelvey has a diverse background in mathematics, software engineering, physical chemistry, and electrochemistry. He obtained his bachelor's and master's degrees in computational modelling from the University of Otago, New Zealand. He designed artificial intelligence and physical simulation solutions for 3D character animation at NaturalMotion. Subsequently, he completed his PhD in Electrochemistry & Interfaces Group at the University of Warwick, UK. His research interests involve studying the impact of nanoscale structure on electrocatalytic reactions and developing experimental techniques to make nanoscale electrochemical measurements. Dr. McKelvey is also involved in integrating nanostructure into energy storage and conversion technologies that are essential for transitioning to a low-carbon economy. He has held various positions in universities in the UK, USA, and New Zealand, and currently works as a Senior Lecturer at Victoria University of Wellington.



NS: Dr. McKelvey, congratulations on your recent outstanding publication on Nature related to electrochemical charge storage mechanism with MXene. Furthermore, you have an impressively diverse academic and professional background. How have these experiences influenced your research interests in electrochemistry and nanoscale structures?

McKelvey:

Thank you. I've always worked at the interface between industry and academia or between different disciplines. Electrochemistry involves oxidation or reduction reactions at a solid-liquid interface, and so I am again working

at an interface. I am interested in electrochemistry because it has so many exciting applications, from batteries to supercapacitors, fuel cells and power-to-X technologies, that are central to using renewable electrical energy for the transition to a low-carbon world.

NS: What experimental techniques have you developed to make nanoscale electrochemical measurements, and what challenges have you faced in implementing them?

McKelvey:

I have been involved in developing several new techniques for mapping chemical and electrochemical reactions at the

nanoscale. These include Intermittent Contact-Scanning Electrochemical Microscopy, dual-electrode and quadruple electrode scanning probes, surface-charge mapping using Scanning Ion Conductance Microscopy, and Bias Modulated Scanning Ion Conductance Microscopy. I have been involved in the development of Scanning Electrochemical Cell Microscopy (SECCM) starting during my time at the University of Warwick working with the brilliant Professor Pat Unwin.

In terms of challenges for developing new experimental scanning probe approaches, the first one is probe fabrication. Ideally you want an approach where the probes are simple and quick to fabricate. The

second challenge is data interpretation. When developing a new experimental electrochemical technique, you need to understand what your electrochemical signal means and what this says about the underlying chemical reactions that are happening at the sample surface.

NS: What principal tools do you use for your nanoscale electrochemistry research and how are they used?

McKelvey:

There are multiple ways to make electrochemical measurements at the nanoscale, from nano impact measurements of single nanoparticles to resistive pulse sensing. The key to all these approaches is being able to restrict the measurement to a nanoscale domain either in space or time. The principal tool I use is Scanning Electrochemical Cell Microscopy. This approach uses a very small droplet at the end of a probe to restrict measurements to very small regions of a sample surface.

Scanning Electrochemical Cell Microscopy has proved to be very versatile, and I am still discovering new things we can use this approach for.

NS: What inspired you to conduct nanoscale electrochemical measurements in this unique experimental configuration, and what challenges did you face during the experiment?

McKelvey:

MXene materials have many interesting electrochemical applications. But MXenes have typically been studied on a large scale, with many individual MXene flakes studied at the same time. We asked ourselves what the intrinsic pseudocapacitive response of a MXene surface was and if we could measure it. Using a Scanning Electrochemical Cell Microscopy approach, we isolated the pseudocapacitive response from a single monolayer flake of MXene. The key challenge we faced in doing

these measurements was locating an appropriate single monolayer flake on our sample surface.

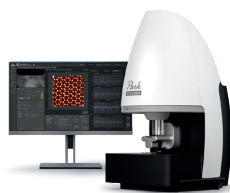
NS: How do you see the field of electrocatalysis evolving in the next 5-10 years, and what potential breakthroughs or advancements do you anticipate in this area?

McKelvey:

Electrolysis technologies are central to reaching zero-carbon, allowing synthesis of chemical products and liquid fuels from renewable electrical energy. With the dropping price of renewable electrical energy, I hope electrolysis technologies (which incorporate nanostructured electrodes) become cost competitive to existing fossil-fuels derived products in the next 10 years. After which, I would hope to see the rapid adoption of electrolysis technologies for the synthesis of a wide range of chemical commodities.



Accelerate Your Research!



Park FX40

A New Class of Atomic Force Microscope

Boost your progress and scientific discoveries through unprecedented speed and accuracy – as the Park FX40 autonomously images and acquires data powered by its artificial intelligence, robotics and machine learning capability.

parksystems.com/fx40



CHARACTERIZATION OF 2D MATERIALS BY IMAGING SPECTROSCOPIC ELLIPSOMETRY (ISE)

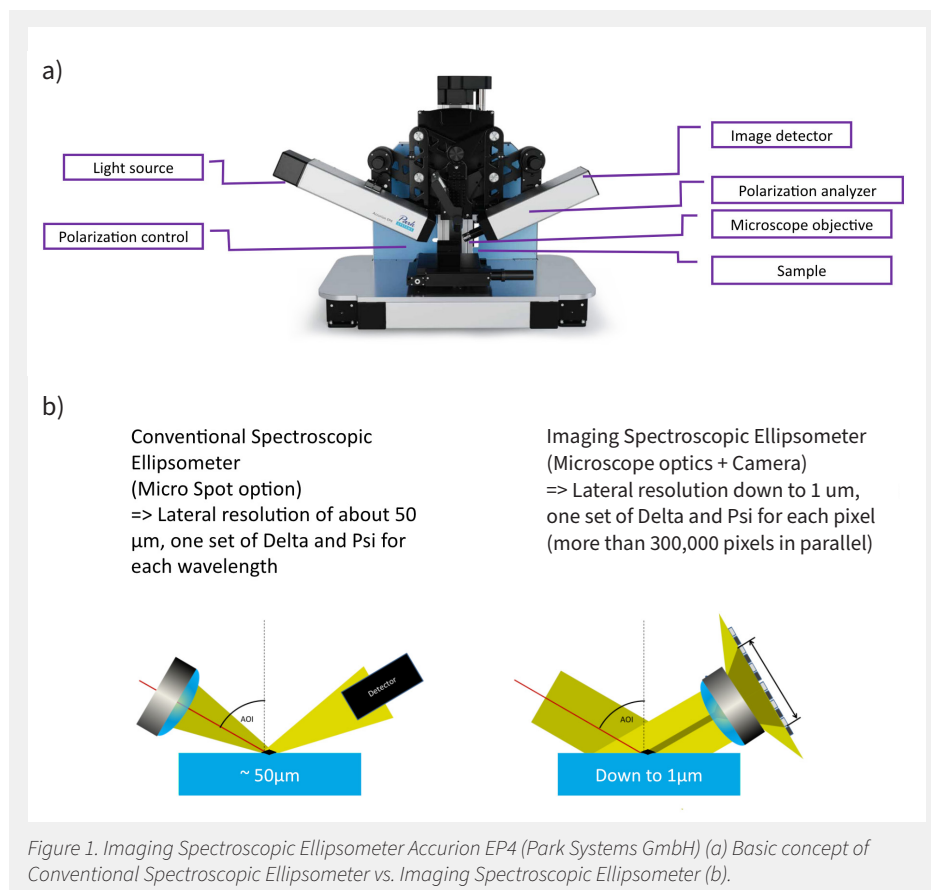
Peter H. Thiesen, Application Specialist, Park Systems GmbH, Accurion Division

Introduction

2D materials, which have the potential to revolutionize entire areas of technology, require decisive tasks to advance developments quickly and efficiently. These tasks include the targeted finding of suitable candidates, as well as fast and efficient quality control of technically manufactured 2D materials. Many scientists especially see applications in the field of micro photonics, lighting, imaging, and sensors. For this range of applications, detailed knowledge of the optical properties is essential, especially to the samples depending on their thickness.

Imaging Spectroscopic Ellipsometry (ISE) is a single device that combines the benefits of spectroscopic ellipsometry and optical microscopy (Figure 1a). The combination of these two technologies creates a unique metrology tool that redefines the limits of both ellipsometric measurements and polarization-contrast microscopy. The enhanced spatial resolution of imaging ellipsometers (down to 1 μm) expands ellipsometry into new areas of microanalysis, microelectronics, and bioanalytics. ISE is an all-optical, non-contact metrology technique that excels in the layer-thickness and material characterization of micro-structured thin-film samples and substrates. The microscopic part allows for a simultaneous measurement of all structures within the field of view of the optical system (Figure 1b). The lateral resolution is defined by the ability of the microscopic part to distinguish details of a specimen or sample, not by the spot size of the illumination beam as in conventional spectroscopic ellipsometry. This provides the benefit of lateral resolution and the capability to use each pixel of the camera as a single detector. Additionally, the detector always offers a live image (ellipsometric contrast micrograph) of the sample, even during the measurement.

In technical applications, the thickness



of a sheet or plate is typically measured using a caliper. To improve the precision of such measurements, a Vernier scale is often employed. In essence, an ellipsometer can be thought of as a Vernier scale for the nano-scale world, with the elliptical polarization state providing a greater degree of accuracy for very thin films – similar to the way in which a Vernier scale is used in macroscopic settings. An imaging ellipsometer merges this thin film metrology tool with microscopic imaging, mapping, and the characterization of microscopic thin films like 2D materials.

The ellipsometric configuration of the Accurion EP4 involves a Polarizer Compensator Sample Analyzer (PCSA), with all optical components being motor-driven. By adjusting the orientation of one or more optical components, the

contrast can be optimized (as shown in Figure 2a), such as between the substrate and a monolayer or between stacks with different layer numbers [1]. Wurstbauer et al. [2010] also demonstrated the ability to optimize contrast between either graphene and substrate or between substrate and impurities from the tape used in exfoliation [2].

Ellipsometric contrast micrographs: Fast, non-contact, wafer-scale, atomic layer resolved imaging with tunable contrast

In general, ellipsometric contrast micrographs (ECM) enable an atomic layer resolved, quantitative mapping of chemical vapour deposited graphene layers on Si/SiO₂-wafers, but also on rough Cu catalyst foils (Figure 2b). Braeuninger-Weimer et al. [2018] highlight

that ECM is applicable to all application relevant substrates and discuss the optimization of ECM parameters for high throughput characterization. Furthermore, they show ECM of mono-layer hexagonal BN (h-BN) and of h-BN/graphene bilayers, highlighting that ECM is applicable to a wide range of 2D layered structures that have been very challenging to characterize before [1].

The shape of an ellipse is defined by Delta and Psi

Ellipsometry deals with elliptic polarized light (Figure 3a) that can be described by the ellipsometric angles Delta and Psi (Figure 3b). Braeuninger- Weimar et al. showed that an even better distinction between the different numbers of layers can be achieved with microscopic delta maps [1].

From the point of view of thin film metrology, it is important that these angles are related by the Drude equation (Figure 3c) with the reflection coefficients of the sample surface. To translate the measured data into physical meaningful parameters like layer thickness of thin films or refractive index of a material, a comparison by a liberation process of the measured data with simulated data is required (optical modelling).

Automated search of flakes of mono- or n-layers of 2D-materials

The aforementioned capability of ECM and Delta-maps to identify samples of specific layer numbers can automatically localize regions of desired thicknesses, such as monolayers or bilayers on any substrate [5]. This process is a promising first step in a cascade of characterization methods from macro to nano. The visualization of defects and grain boundaries in large-area graphene coatings using an ECM/Delta maps-based QC approach, in combination with complementary technologies like atomic force microscopy (AFM) and magnetic force microscopy (MFM), is especially promising.

Micro Ellipsometry versus Microscopic

The capability of imaging ellipsometry can be explained by using two borderline cases. The first method is micro ellipsometry, where optical thin-film metrology is based on so-called regions of interest (ROI). These ROIs are set to select the camera pixels that are averaged for the measurement. The

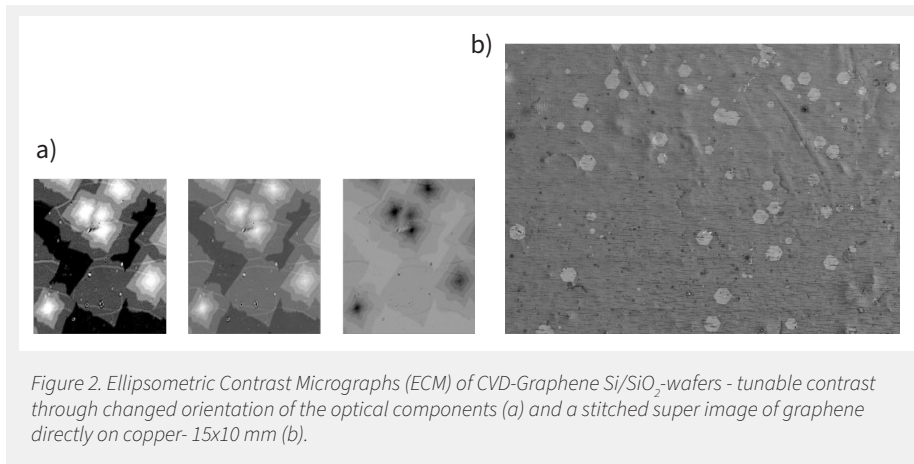


Figure 2. Ellipsometric Contrast Micrographs (ECM) of CVD-Graphene Si/SiO₂-wafers - tunable contrast through changed orientation of the optical components (a) and a stitched super image of graphene directly on copper- 15x10 mm (b).

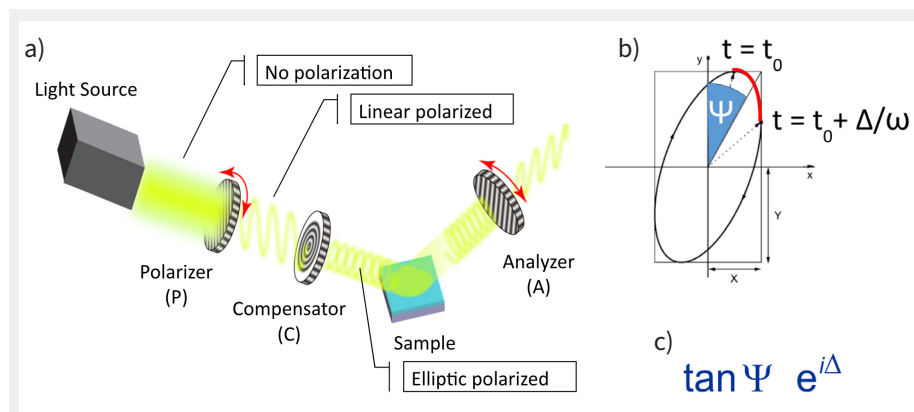


Figure 3. Change of the state of polarization on the pathway of light of an ellipsometer (a) [3], [4] and how the shape of an ellipse is described by the ellipsometric angles Delta and Psi (b) and Drude equation (c).

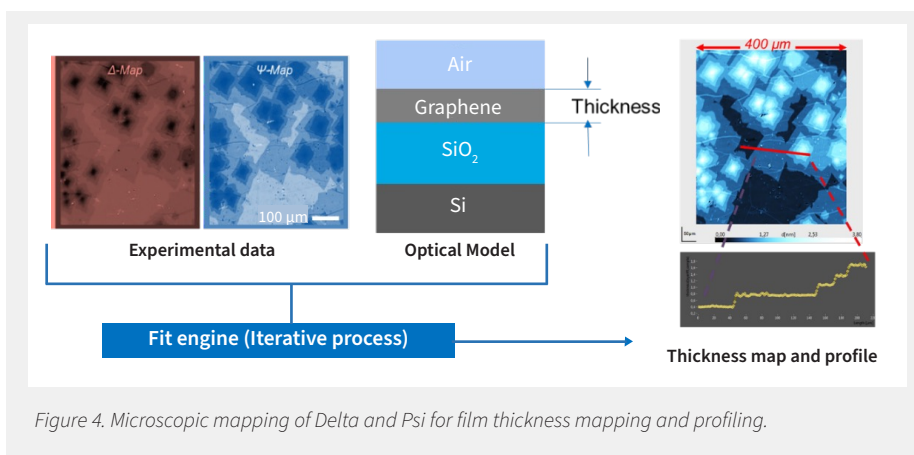


Figure 4. Microscopic mapping of Delta and Psi for film thickness mapping and profiling.

second method is microscopic mapping, which involves determining parallel values for all the pixels, thereby enabling the determination of a layer thickness map or distribution.

Optical dispersion of 2D-Materials

Let's examine the spectroscopic ability of ISE in more detail: The main goal of spectroscopic ellipsometry measurements for 2D materials is to determine the optical characteristics of the flakes. The acquired data involves comparing the sets of delta and Psi measurements (for each ROI or even

per pixel) with calculated values of an optical model through an iterative process. The calculation is founded on the overall layer structure. The optical properties of the substrate are predetermined or preferably, determined simultaneously - a standard technique in the characterization of 2D materials using an imaging ellipsometer. In the literature, optical dispersion detection based on ISE has been reported for various materials, including graphene [6], graphene oxide [7], graphene embedded in h-BN [8], 2D-MoS₂ [9],[10], 2D-MoO₃ [11], and TCM-

heterostructure [12] – just to name a few. The next step could be determining the shape, size, and symmetry of these materials depending on their optical properties [13]. For a more general outlook on future limitations and requirements, please refer to the paper titled "Imaging ellipsometry for structured and plasmonic materials" [14].

Operando Imaging Spectroscopic Ellipsometry

Over the past few years, several papers have been published on operando imaging ellipsometry [15] and operando imaging spectroscopic ellipsometry [16] of graphene-based samples. The key aspect is that imaging ellipsometry can detect changes in the thin film material during processes. For instance, it can track the intercalation of sodium ions depending on the voltage.

Conclusion

In conclusion, Imaging Spectroscopic Ellipsometry (ISE) proves to be a powerful tool for the characterization of 2D materials, filling an important gap in 2D metrology. It can be utilized to measure the thickness of monolayers, as well as the optical properties of 2D materials. Additionally, it is applicable for measuring heterostructures and small devices, as well as identifying defects and wrinkles in the flakes. Moreover, it can measure the optical properties of 2D materials on various substrates, making Imaging Ellipsometry a valuable tool for the characterization of 2D materials.

References:

[1] Braeuninger-Weimer, P., Funke, S., Wang, R., Thiesen, P., Tasche, D., Viöl, W., & Hofmann, S. (2018). Fast, noncontact, wafer-scale, atomic layer resolved imaging of two-dimensional materials by ellipsometric contrast micrography. *Acs Nano*, 12(8), 8555-8563.

[2] Wurstbauer, U., Röling, C., Wurstbauer, U., Wegscheider, W., Vaupel, M., Thiesen, P. H., & Weiss, D. (2010). Imaging ellipsometry of graphene. *Applied Physics Letters*, 97(23), 231901.

[3] Operation Manual EP4, Park systems

[4] Tompkins, H., & Irene, E. A. (2005). *Handbook of ellipsometry*. William Andrew.

[5] Funke, S., Wurstbauer, U., Miller, B., Matković, A., Green, A., Diebold, A., ... & Thiesen, P. H. (2017). Spectroscopic imaging ellipsometry for automated search of flakes of mono- and n-layers of 2D-materials. *Applied Surface Science*, 421, 435-439.

[6] Matković, A., Beltaos, A., Miličević, M., Ralević, U., Vasić, B., Jovanović, D., & Gajić, R. (2012). Spectroscopic imaging ellipsometry and Fano resonance modeling of graphene. *Journal of Applied Physics*, 112(12), 123523.

[7] Jung, I., Vaupel, M., Pelton, M., Piner, R., Dikin, D. A., Stankovich, S., ... & Ruoff, R. S. (2008). Characterization of thermally reduced graphene oxide by imaging ellipsometry. *The Journal of Physical Chemistry C*, 112(23), 8499-8506.

[8] Toksumakov, A. N., Ermolaev, G. A., Tatmyshevskiy, M. K., Klislin, Y. A., Slavich, A. S., Begichev, I. V., ... & Ghazaryan, D. A. (2023). Anomalous optical response of graphene on hexagonal boron nitride substrates. *Communications Physics*, 6(1), 13.

[9] Funke, S., Miller, B., Parzinger, E., Thiesen, P., Holleitner, A. W., & Wurstbauer, U. (2016). Imaging spectroscopic ellipsometry of MoS₂. *Journal of Physics: Condensed Matter*, 28(38), 385301.

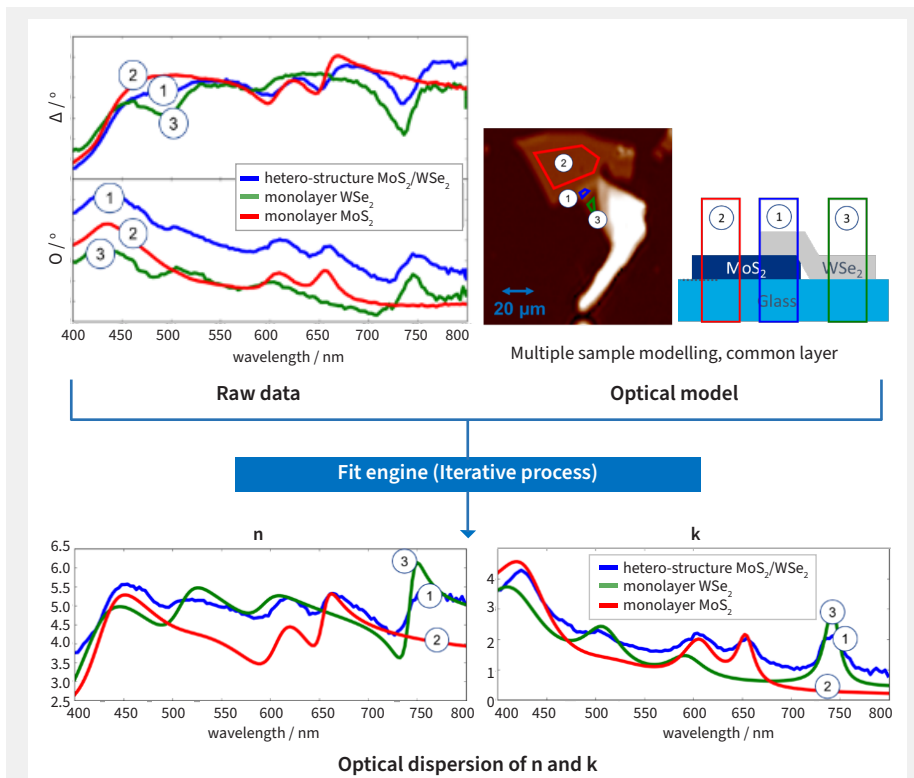


Figure 5. Micro ellipsometry of a heterostructure of 2D-materials using different regions of interest (ROI) in parallel (1),(2),(3).

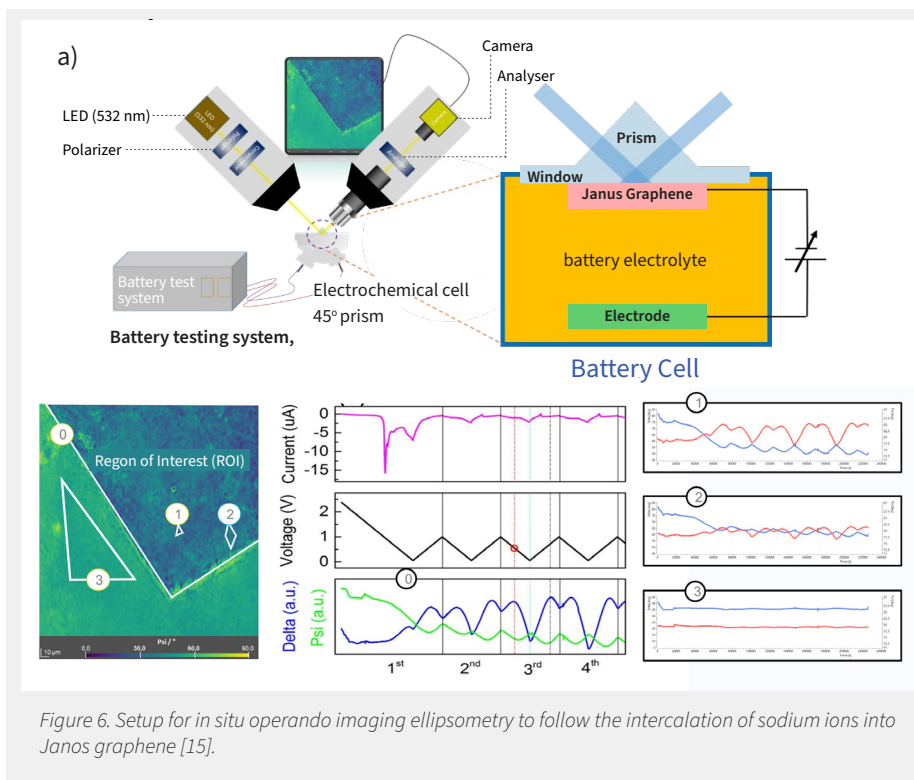


Figure 6. Setup for in situ operando imaging ellipsometry to follow the intercalation of sodium ions into Janos graphene [15].

[10] Ermolaev, G. A., Stebunov, Y. V., Vyshnevyy, A. A. et al. (2020) Broadband optical properties of monolayer and bulk MoS₂. *npj 2D Mater Appl* 4, 21 (2020). <https://doi.org/10.1038/s41699-020-0155-x>

[11] Andres-Penares, D., Brotons-Gisbert, M., Bonato, C., Sánchez-Royo, J. F., & Gerardo, B. D. (2021). Optical and dielectric properties of MoO₃ nanosheets for van der Waals heterostructures. *Applied Physics Letters*, 119(22), 223104.

[12] Sigger, F., Lambers, H., Nisi, K., Klein, J., Saigal, N., Holleitner, A. W., & Wurstbauer, U. (2022). Spectroscopic imaging ellipsometry of two-dimensional TMDC heterostructures. *Applied Physics Letters*, 121(7), 071102.

[13] Magnozzi, M., Pflug, T., Ferrera, M., Pace, S., Ramó, L., Olbrich, M., ... & Canepa, M. (2021). Local optical properties in CVD-grown monolayer WS₂ flakes. *The Journal of Physical Chemistry C*, 125(29), 16059-16065.

[14] Hingerl, Kurt. "Imaging ellipsometry for structured and plasmonic materials." *Journal of Applied Physics* 129.11 (2021): 113101.

[15] Sun, J., Sadd, M., Edenberg, P., Grönbeck, H., Thiesen, P. H., Xia, Z., ... & Palermo, V. (2021). Real-time imaging of Na⁺ reversible intercalation in "Janus" graphene stacks for battery applications. *Science advances*, 7(22), eabf0812.

[16] Okano, S., Sharma, A., Ortman, F., Nishimura, A., Günther, C., Gordan, O. D., ... & Zahn, D. R. (2020). Voltage-controlled dielectric function of bilayer graphene. *Advanced optical materials*, 8(20), 2000861.

FUNCTIONAL POLYMERIC PASSIVATION-LED IMPROVEMENT OF BIAS STRESS WITH LONG-TERM DURABILITY OF EDGE-RICH NANOPOROUS MoS₂ THIN-FILM TRANSISTORS

Heekyeong Park (Harvard University, USA), Junhwan Choi (KAIST, Republic of Korea), Junoh Shim (SKKU, Republic of Korea), Seung Min Lee (KAIST, Republic of Korea), Sungmin On (Pohang Accelerator Laboratory, Republic of Korea), Hyung Joong Yun (KBSI, Republic of Korea), Sunkook Kim (SKKU, Republic of Korea), Sung Gap Im (KAIST, Republic of Korea), Hocheon Yoo (Gachon University, Republic of Korea).

This article has been condensed under Creative Commons Attribution License www.nature.com/articles/s41699-022-00296-7

Abstract

Nanoporous patterning of two-dimensional materials using block copolymer (BCP) lithography has drawn much attention. Lateral edge exposures made by the nanoporous patterning provide electrical and optical characteristics that are different from the original materials. However, nanopatterning processes inevitably generate edge exposure and surface defects that may result in poor reliability and reproducibility of the devices. This study proposes a reliable method to passivate nanoporous molybdenum disulfide (MoS₂) thin-film transistors (TFTs) using polymer thin films, synthesized by initiated chemical vapor deposition (iCVD), to improve the electrical stability of nanoporous MoS₂ TFTs. Functional polymer films of electron-donating poly(1-vinylimidazole) (pVI) and inert poly(1H,1H,2H,2H-perfluorodecyl methacrylate) (pPFDMA) were utilized as passivation layers on nanoporous MoS₂ TFTs. The superior passivation effect of the pPFDMA layer was confirmed using gate-bias stress tests and long-term storage tests under ambient conditions.

Introduction

2D materials have high carrier mobility, sharp subthreshold slope, and great

endurance to mechanical stress, making them ideal for functional electronics, such as flexible TFTs and ICs. Their large surface-to-volume ratio has enabled the development of phototransistors, gas sensors, and biosensors. 2D materials' electrical and optical properties can be tuned using structural engineering, making them ideal for electronic devices. Modifying dimensions or morphology changes structural properties, imparting exotic properties to overcome material limitations. For example, the graphene TFTs modified to form nanodot, nanoribbon, and nanomesh have finite bandgaps and superior electrical switching properties. Kim et al* also showed potential to overcome MoS₂'s low photoluminescence with an indirect bandgap by patterning 2D materials to nanopore sheets.

BCP lithography is a simple, cost-effective way to create nanostructured 2D materials with regular nanosized features. These materials have lateral edge exposures that pristine 2D materials lack, allowing for unique properties and applications such as optoelectronics, chemical/biomedical sensing, and catalytic activity. Nanopatterning can improve device performance. However, nanopatterning of 2D materials has a severe disadvantage: edge exposure and structural defects lead to electrical instability due to oxygen and moisture adsorption. This affects device characteristics and causes hysteresis. Passivation of the nanopatterned surface is essential to prevent external contaminants.

Various inorganic and organic layers have been used to passivate 2D materials via atomic layer deposition (ALD), pulsed laser deposition, and solution-based deposition. However, these methods can damage and degrade the channel surface, affecting the electrical performance of nanopatterned TFTs due to unstable edges and defects being susceptible to high temperatures and solvents.

The polymeric passivation of a nanopatterned MoS₂ TFT via iCVD, a vapor-phase process that enables solvent-free, was used near-room-temp deposition of polymer thin films without damaging the underlying 2D materials. Conformal coverage is challenging in conventional ALD and solution-based deposition, but iCVD can deposit ultrathin polymer films conformally on any 2D material surface from the input monomers adsorbed thereon.

The pVI and pPFDMA polymer films were used to passivate nanoporous MoS₂ TFTs. The polymer layers and electrical/chemical changes were confirmed using Raman spectroscopy, ultraviolet photoelectron spectroscopy (UPS), scanning transmission electron microscopy (STEM), X-ray photoelectron spectroscopy (XPS), atomic force microscopy (AFM), and current measurements. Remarkably, pPFDMA layer passivated the MoS₂ under repeated gate-bias stress and long-term air exposure, enabling long-term stable operation of the TFT.

RESULTS

Chemical and morphological properties of nanoporous MoS₂

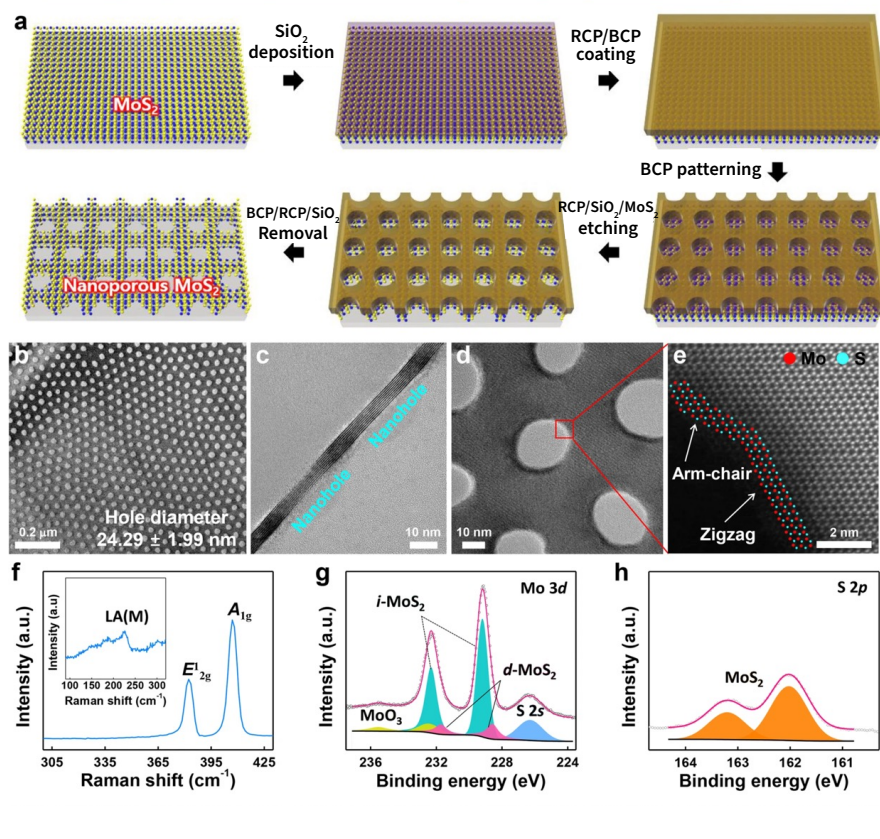
Figure 1 describes a process for fabricating nanoporous MoS₂ using a multilayer MoS₂ film transferred onto a Si/SiO₂ substrate, followed by the self-assembly of a block copolymer layer to create a periodic nanohole pattern, and selective decomposition of the polymer block to obtain the desired nanoporous structure. The resulting nanoporous MoS₂ was characterized using various analytical techniques, such as STEM, Raman spectroscopy, and XPS, which revealed its morphological and chemical properties.

Polymeric passivation of nanoporous MoS₂

Figure 2 shows a schematic of the polymer deposition process on the nanoporous MoS₂ surface. The polymeric passivation layers, specifically pVI and pPFDMA are used on nanoporous MoS₂ surfaces using the iCVD process. The process allows for solvent-free deposition at a low temperature, which minimizes damage to the substrate surface. The resulting polymer films preserve the chemical functionalities of the monomers and have distinct electrical properties. Raman spectroscopy and UPS analyses were performed to investigate the variation in the electrical characteristics of the nanoporous MoS₂ films with each polymer passivation layer. The pVI passivation layer induced an n-doping effect, while the pPFDMA passivation layer induced an insignificant p-doping effect. The electrical effects of the two polymer layers were observed to be highly coherent on both nanoporous and non-patterned MoS₂ films.

Characterization of polymer-passivated nanoporous MoS₂ film

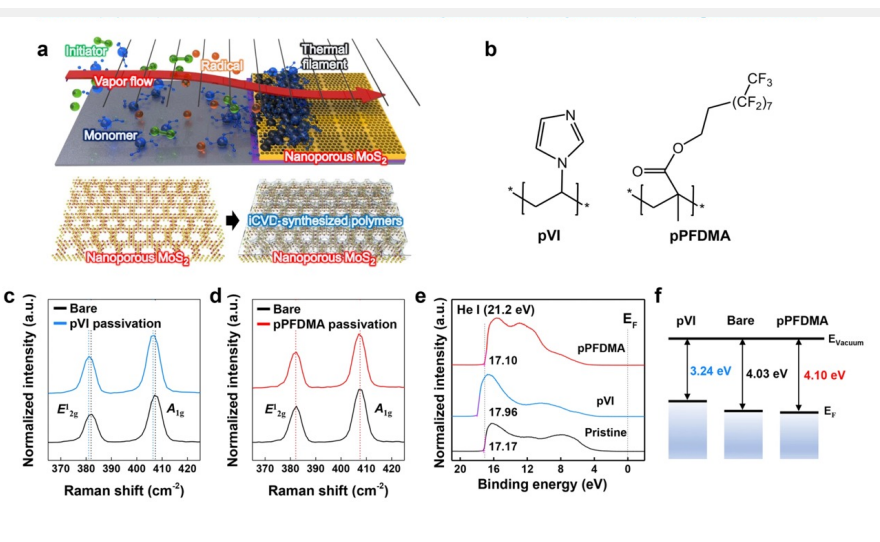
In figure 3, the study used high-angle annular dark-field (HAADF)-STEM analysis to confirm the effective passivation of two different polymer layers on nanoporous MoS₂. The cross-sectional HAADF-STEM images with energy dispersive spectroscopy (EDS) mapping showed that both polymer layers were deposited conformally on the surface without notable defects.



a Schematic illustration of the fabrication process of nanoporous MoS₂. **b** Low-magnification STEM image and **c** cross-sectional view of nanoporous MoS₂. **d** STEM image representing the hexagonally packed nanohole array. **e** Atomic configuration of the exposed edge in nanoporous MoS₂. **f** Raman and **g**, **h** XPS spectra of nanoporous MoS₂.

Figure 1: Fabrication and observation of nanoporous MoS₂ film.

From: *Functional polymeric passivation-led improvement of bias stress with long-term durability of edge-rich nanoporous MoS₂ thin-film transistors*



a Schematic illustration of the passivation of nanoporous MoS₂ by iCVD process and **b** chemical structures of passivation layers. **c**, **d** Raman spectra and **e** UPS spectra of the pI- and pPFDMA-passivated nanoporous MoS₂, compared to the pristine one. **f** Energy band structures of the polymer-passivated nanoporous MoS₂ compared to the pristine one calculated from the UPS analysis.

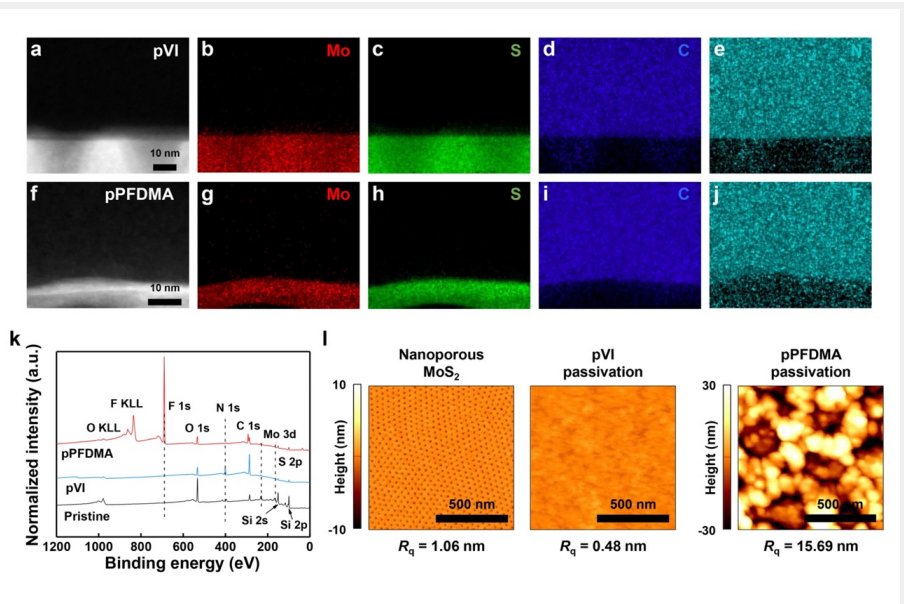
Figure 2: Polymeric passivation of nanoporous MoS₂ films using pI and pPFDMA respectively.

From: *Functional polymeric passivation-led improvement of bias stress with long-term durability of edge-rich nanoporous MoS₂ thin-film transistors*

The surface chemical composition of the polymer-passivated nanoporous MoS₂ was investigated by XPS and compared with pristine nanoporous MoS₂, showing that the polymer passivation layer conformally covered the nanoporous MoS₂ surface. To further investigate the surface properties of the polymer-passivated nanoporous MoS₂, AFM analysis was performed using a scanning probe microscope (XE-100, Park Systems). The AFM image of the pristine nanoporous MoS₂ clearly exhibited porous structure and the smooth, amorphous surface morphology was confirmed with the root-mean-square roughness (R_q) < 0.5 nm, which also indicates that the pVI layer conformally covered the nanoporous MoS₂. On the other hand, the AFM image of the pPFDMA-passivated nanoporous MoS₂ exhibited the roughened surface with the R_q value > 15 nm. This rough surface morphology was originated from the highly crystalline nature of pPFDMA due to the fluoroalkyl chain, which can also improve the hydrophobicity of the surface. The water contact angle (WCA) analysis also verified that the surface property of the nanoporous MoS₂ was controlled according to the deposition of the polymer films (Supplementary Fig. 7). Therefore, it follows from the comprehensive analyses that the vapor-phase-deposited polymer passivation layers conformally covered the nanoporous MoS₂ surface without incurring defect or damage to the underlying MoS₂, while fully retaining the chemical functionalities of each polymer film.

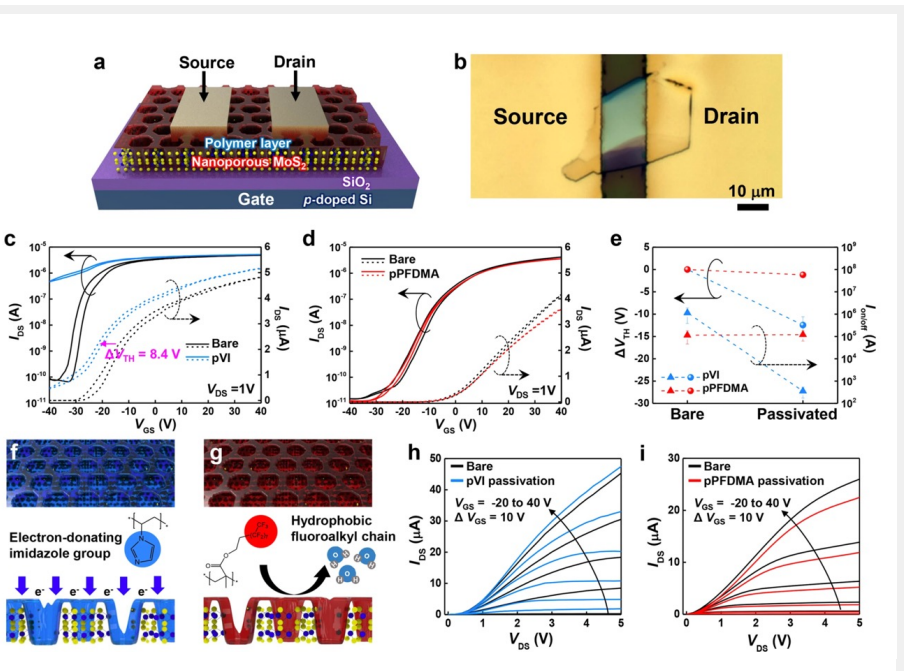
Electrical characteristics of nanoporous MoS₂ TFTs passivated by pVI and pPFDMA polymers

The study investigated the effect of passivation with pVI and pPFDMA layers on the electrical characteristics of nanoporous MoS₂ TFTs, Figure 4. The passivation with both polymer layers effectively prevented charge trapping on the MoS₂ edge-air interface and reduced hysteresis. The pVI layer induced n-doping behavior and a significant increase in the drain current (I_{DS}), while the pPFDMA layer minimally changed the electrical characteristics of the TFTs. The polymer layers had little effect on the carrier scattering at the interface between the nanoporous MoS₂ and the polymer. The output curves showed a more prominent increase IDS in the



HAADF-STEM images and EDS elemental mapping of the **a-e** pVI- and **f-j** pPFDMA-passivated nanoporous MoS₂. False color modification was attempted in EDS elemental mapping images to clearly reveal the polymeric passivation layers and nanoporous MoS₂. **k** XPS survey scan spectra of the pristine and polymer-passivated nanoporous MoS₂. The N1s and F1s peaks were detected only in the VI- and pPFDMA-passivated nanoporous MoS₂. **l** AFM images of the polymer-passivated nanoporous MoS₂ as well as the pristine one.

Figure 3: Chemical and morphological properties of polymer-passivated nanoporous MoS₂ films. From: *Functional polymeric passivation-led improvement of bias stress with long-term durability of edge-rich nanoporous MoS₂ thin-film transistors*



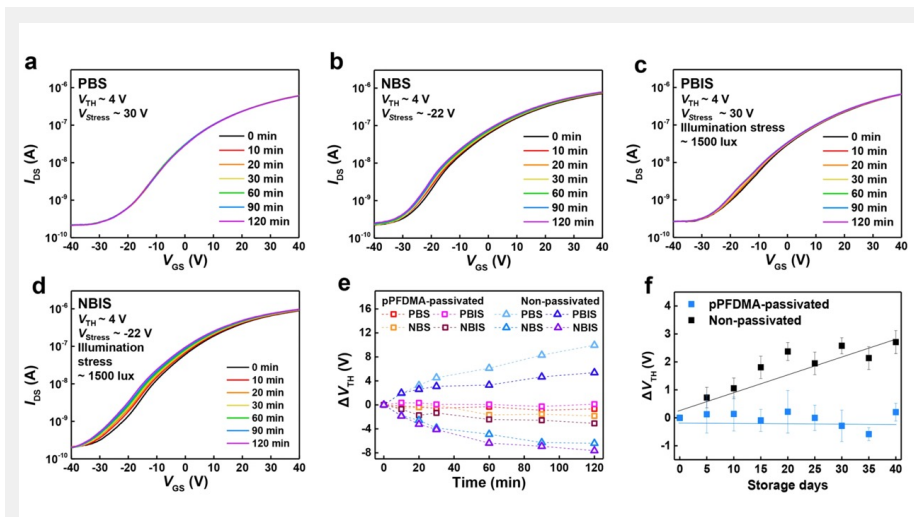
a Schematic and **b** optical images of polymer-passivated nanoporous MoS₂ TFT. Transfer characteristics of the nanoporous MoS₂ TFT before and after deposition of **c** pVI and **d** pPFDMA films. **e** Variation in V_{th} and $I_{on/off}$ of the nanoporous MoS₂ TFTs after passivation with pVI and pPFDMA layers, respectively. Schematic of electrical behavior at polymer/MoS₂ interface when passivated with **f** pVI and **g** pPFDMA layers, respectively. Output curves of **h** pVI- and **i** pPFDMA-deposited nanoporous MoS₂ TFTs together with the corresponding non-passivated TFTs.

Figure 4: Electrical properties of polymer-passivated nanoporous MoS₂ TFTs. From: *Functional polymeric passivation-led improvement of bias stress with long-term durability of edge-rich nanoporous MoS₂ thin-film transistors*

lower range of gate voltage (VGS) for pVI-deposited TFTs and a practically identical shape for pPFDMA-deposited TFTs.

Stability tests of pPFDMA-passivated nanoporous MoS₂ TFTs

Figure 5 shows the passivation effect of the pPFDMA layer grown by iCVD on the nanoporous MoS₂ TFTs. Gate-bias stress tests and long-term storage tests were conducted under ambient air conditions to examine the passivation performance of the pPFDMA layer on the nanoporous MoS₂ TFTs. The results suggest that the pPFDMA passivation layer can effectively prevent the charge trapping induced by the adsorption of oxygen or water in an ambient environment at the edge defect sites. The long-term storage test also confirms the excellent passivation performance of the pPFDMA polymer synthesized by the iCVD process for robust nanoporous MoS₂ devices.



Transfer characteristics of the pPFDMA-passivated nanoporous MoS₂ TFT under **a** PBS, **b** NBS, **c** PBIS, and **d** NBIS conditions with positive bias stress of 30V and negative bias stress of -22 V. A light source of 1500 lux was used for the illumination stress. **e** Variation of V_{TH} of nanoporous MoS₂ TFT passivated with pPFDMA layer and non-passivated one according to the stress time. **f** Long-term storage test of pPFDMA-passivated and non-passivated nanoporous MoS₂ TFTs under exposure in the ambient environment.

Figure 5: Gate bias and illumination stress tests and long-term storage test of pPFDMA-passivated nanoporous MoS₂ TFTs.

From: *Functional polymeric passivation-led improvement of bias stress with long-term durability of edge-rich nanoporous MoS₂ thin-film transistors*

SUMMARY

In summary, the study demonstrates an efficient passivation method for nanoporous MoS₂ using polymeric passivation layers via iCVD process. The proposed solvent-free method effectively passivated the surface edges and defects in nanoporous MoS₂, without damaging or degrading its structure and electrical integrity. The pVI with an electron-donating imidazole ring and pPFDMA containing a fluoroalkyl chain were utilized as n-doping and inert polymer passivation layers, respectively. Both polymer passivation layers conformally covered the underlying nanostructured MoS₂. The nanoporous MoS₂-based TFT with the polymer passivation layers showed a significant negative V_{TH} shift in the pVI-deposited nanoporous MoS₂ TFT, whereas the pPFDMA-deposited nanoporous MoS₂ TFT only exhibited a small reduction in the on-current. On the other hand, the long fluoroalkyl chain in the pPFDMA provided strong hydrophobicity, thus remarkably enhancing the stability of the nanoporous MoS₂ TFT in ambient air. The pPFDMA-deposited nanoporous MoS₂ TFT demonstrated outstanding stability in the PBS, NBS, PBIS, and NBIS tests compared to the non-passivated device, primarily because the pPFDMA

can efficiently abate the water and oxygen adsorption on the nanoporous MoS₂ surface. In addition, only a negligible change was observed in the long-term storage test, which confirms the robustness of the pPFDMA-deposited nanoporous MoS₂ TFT. The study provides an effective strategy for the passivation of nanostructured 2D materials. In particular, a vapor-phase deposited fluoropolymer can enhance the ambient stability of nanostructured 2D materials-based TFTs, without damaging their electrical characteristics.

* Kim, T. et al. Structural defects in a nanomesh of bulk MoS₂ using an anodic aluminum oxide template for photoluminescence efficiency enhancement. *Sci. Rep.* 8, 1–6
This article has been condensed under Creative Commons Attribution License.
The complete article including all references can be found here: www.nature.com/articles/s41699-022-00296-7

2023 NANOScientific Symposium

Connecting the Nanoscience Community

Register Now!

event.nanoscientific.org



HOW TO TAILOR THE CRYSTALLOGRAPHIC ORIENTATION EVOLUTION AND SURFACE MORPHOLOGICAL FEATURES OF POLYCRYSTALLINE CONDUCTIVE N-TYPE ZNO FILMS

Tetsuya Yamamoto, Research Institute, Kochi University of Technology, Japan

Introduction

Highly transparent conductive oxide (TCO) films, such as n-type In_2O_3 - and ZnO-based films, are of great interest for use as transparent conducting electrodes in optoelectronic devices (e.g., photovoltaic solar cells and flat display panels [1-4]). It is essential to adjust the trade-off between optical transparency and electrical conductivity to meet the requirements of various applications. Recently, atomic force microscopy (AFM: Park Systems NX10) has been used to analyze the data from a two-step film growth technique [5-8]. It has demonstrated to be an effective way of improving the electrical properties and tailoring the texture and surface morphology of transparent conductive Al-doped ZnO (AZO) polycrystalline films. Therefore, AZO films are a promising alternative to the commonly used Sn-doped In_2O_3 (ITO), as Al and Zn are cheap, nontoxic and abundant raw materials.

It is well known that the electrical and optical properties of polycrystalline AZO films strongly depend on film-growth methods. The conventional and representative film-growth methods are direct current (dc) magnetron sputtering (dc-MS) [9] or radio frequency (rf) MS (rf-MS) [9]. Although dc-MS has the advantage of higher film-growth rates over rf-MS from a production standpoint, there are still issues that need to be resolved. RF-magnetron-sputtered AZO (rf-MS-AZO) polycrystalline films

deposited on the amorphous glass substrates have a texture with a well-defined (0001) orientation (see Figure 1) [6,7]. On the other hand, polycrystalline AZO films deposited by dc-MS have a texture with a mixed orientation of the (0001) plane with other planes, such as (10-11), (20-21) and (30-32) (see Figure 1)) [6,7]. This leads to a large contribution of grain boundary (GB) scattering to carrier transport compared with rf-MS-AZO polycrystalline films, resulting in a reduced Hall mobility (μ_{H}).

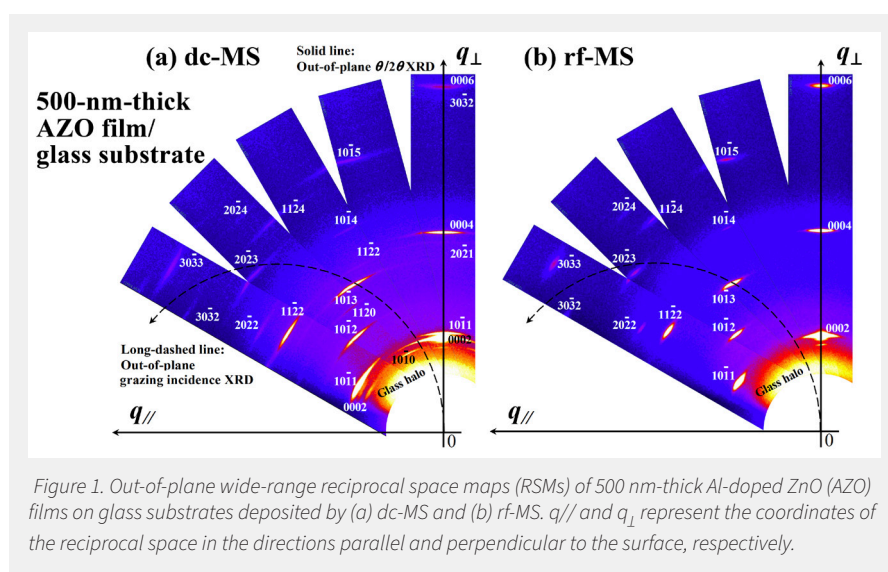


Figure 1. Out-of-plane wide-range reciprocal space maps (RSMs) of 500 nm-thick Al-doped ZnO (AZO) films on glass substrates deposited by (a) dc-MS and (b) rf-MS. $q_{//}$ and q_{\perp} represent the coordinates of the reciprocal space in the directions parallel and perpendicular to the surface, respectively.

The presence of the above GB in polycrystalline films reduces carrier transport, as evidenced by Hall effect measurements which show μ_{H} to be lower than the intrinsic carrier mobility in grains determined by optical measurements [10,11]. Additionally, dc-magnetron-sputtered AZO (dc-MS-AZO) films deposited on amorphous glass substrates have a high average roughness (R_{a}) compared with rf-MS-AZO films deposited on amorphous glass substrates at any given film thickness, as seen in Figs. 2 and 3. In such films, lowered visible optical transmission are observed. To address these issues, we have developed a technology in which a 10 nm-thick rf-MS-AZO film, referred to as a critical layer, is inserted at the dc-MS-AZO film/substrate interface; It is essential that this critical layer has a feature of texture showing a preferential c-axis orientation on amorphous glass substrates.

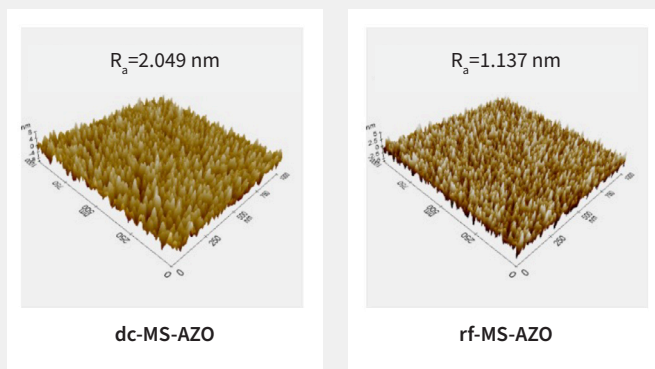


Figure 2. AFM images of (a) a 50 nm-thick dc-MS-AZO film on a glass substrate and (b) a 50 nm-thick rf-MS-AZO film on a glass substrate.

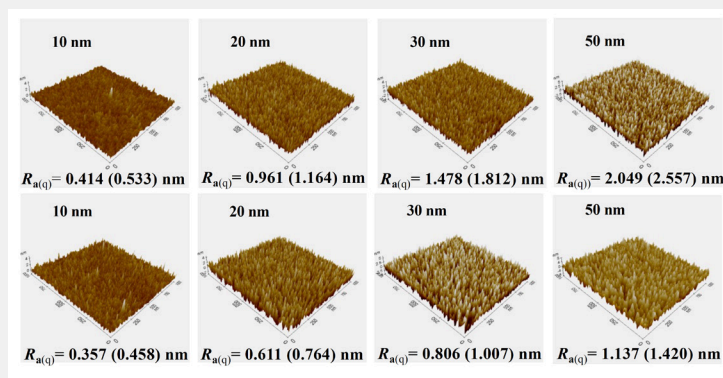


Figure 3. AFM images of AZO films of various thicknesses deposited on amorphous glass substrates by dc-MS (upper part) and rf-MS (lower part).

Experimental

We deposited AZO films on amorphous glass substrates (Corning Eagle XG) at a substrate temperature of 200 °C using MS apparatus (ULVAC CS-L) with a dc or rf power of 200 W. The oxide targets (Toshiba Manufacturing Corp.) were high-density sintered circular AZO targets (diameter: 80 mm) with an Al₂O₃ content of 2.0 wt. % (3.16 mol.%). To investigate the effects of the critical layer on the surface and electrical properties of dc-MS-AZO films deposited on amorphous glass substrates, four types of samples were prepared [7]. Sample 1 was a 500 nm-thick rf-MS-AZO film on an amorphous glass substrate; sample 2 was a 500 nm-thick dc-MS-AZO film on the glass substrate; for sample 3, we first a 10 nm-thick rf-MS AZO film on the glass substrate as the critical layer, followed by a 490 nm-thick dc-MS AZO film; for sample 4, we first deposited a 10 nm-thick dc-MS-AZO film on the glass substrate as the critical layer, on which we subsequently deposited a 490 nm-thick rf-MS-AZO film. The temperature of the amorphous glass substrate was fixed at 200 °C for all deposition processes of samples. For a comprehensive analysis of the textures of the thick AZO films, we conducted out-of-plane wide-range reciprocal space maps (RSMs) measurements using a SmartLab XRD system (Rigaku Corp.) equipped with a PILATUS 100K/R two-dimensional X-ray detector and Cu K α radiation (wavelength $\lambda = 0.15418$ nm, based on the weighted average of Cu K α_1 ($\lambda = 0.154059$ nm) and Cu K α_2 ($\lambda = 0.15444$ nm) in an intensity ratio of 2:1) [12]. The surface morphology was analyzed by AFM (Park Systems NX10) [13], with a scan area and speed of 1 \times 1 μm^2 and

2 $\mu\text{m/s}$ (1 Hz scan rate), respectively. R_a , root-mean-square roughness (R_q) and surface kurtosis (R_{ku}) were used to evaluate the surface morphology of the AZO films deposited directly on the glass substrates or on the glass substrates with the critical layer. The electrical properties, carrier concentration (n_e), μ_{H} and electrical resistivity (ρ), were determined at room temperature by Hall effect measurements in a van der Pauw geometry (Nanometrics, HL5500PC).

Results and Discussion

Figure 3 displays AFM images of AZO films with various thicknesses deposited on amorphous glass substrates by dc-MS (upper part) and rf-MS (lower part). In Figure 3, we indicate R_q and R_a in all the films. The ratio of R_q to R_a is almost 1.25 for rf-MS-AZO films with thicknesses of more than 20 nm [7], indicating that such films have surfaces with a Gaussian height distribution (theoretical value is $\sqrt{\pi/2}$) [14,15]. 10 nm-thick dc-MS and rf-MS-AZO films had R_{ku} of more than 3, which suggests a spikey surface with a large number of high peaks and low valleys [14]. The rf-MS-AZO films with thicknesses of 20 nm or more had R_{ku} of 3, which indicates a perfectly random surface [14]. On the other hand, for dc-MS-AZO films, R_{ku} was below 3 regardless of the thickness, suggesting a bumpy surface with few high peaks and low valleys. This can prevent the lateral growth caused by the sufficient migration of adatoms such as Zn, Al and O atoms from one grain to adjacent grains; bumps located at higher surface positions may grow faster at the expense of other valleys, leading to the enhanced surface roughness shown in Figure 3. In such films, poor additional lateral relaxation

processes during film growth will inevitably cause dynamic roughening, i.e., the surface roughness increases as the thickness increases (see Figure 4). Figure 4 shows R_q of AZO films with thicknesses ranging from 10 to 50 nm deposited on amorphous glass substrates by dc-MS or rf-MS. It is evident that R_q of dc-MS-AZO films show a sharp increase compared with rf-MS-AZO films with increasing the film thickness.

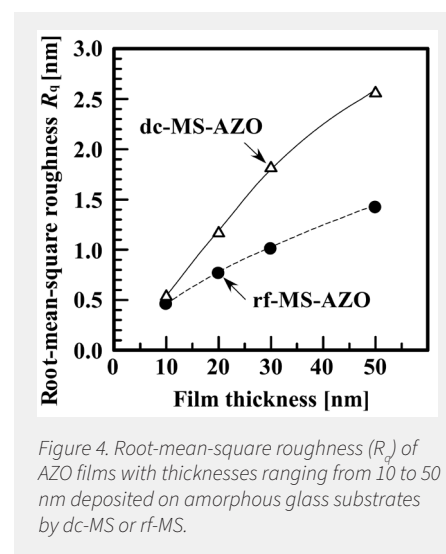


Figure 4. Root-mean-square roughness (R_q) of AZO films with thicknesses ranging from 10 to 50 nm deposited on amorphous glass substrates by dc-MS or rf-MS.

In Table 1, we summarized the surface properties and lateral grain sizes calculated using the data determined from in-plane XRD measurements of each sample. Figure 5 shows cross-sectional schematic diagrams, AFM images and out-of-plane wide-range RSMs of samples 2 and 3. The results in Figure 5 and Table 1 demonstrate that the use of 10 nm-thick critical layers composed of rf-MS-AZO films deposited on amorphous glass substrates drastically reduced R_a and R_q of 490 nm-thick dc-MS-AZO films grown on the critical layers (sample 3) compared with those of the

other samples, particularly 500 nm-thick dc-MS-AZO films deposited on amorphous glass substrates (sample 2). The top and bottom out-of-plane wide-range RSMs in Figure 5 demonstrate that the postannealing-free technology using only very thin critical layers yields thick dc-MS-AZO films with a texture featuring a well-defined (0001) crystallographic orientation between columnar grains, resulting in the formation of small-angle grain boundaries. This leads to an increase in n_e by 6.76 % and μ_H by 15 % compared with thick AZO films deposited on critical-layer-free glass substrates, resulting in a decrease in ρ , which is inversely proportional to the product of n_e and μ_H , by 18.3 % ($\rho = 2.32 \times 10^{-4} \Omega\text{cm}$). The improvement of μ_H is attributed to the fact that the GB scattering mechanism contributes very little to the carrier transport.

Table 1. Root-mean-square roughness (R_q), average roughness (R_a), ratio (R_q/R_a) of R_q to R_a , surface kurtosis (R_{ku}) and lateral grain size (L) of Samples 1-4. See text (Experimental section) for details of each sample.

	R_q (nm)	R_a (nm)	R_q/R_a	R_{ku}	L (nm)
sample 1	7.55	6.15	1.23	2.62	42.84
sample 2	8.17	6.64	1.23	2.72	44.06
sample 3	5.02	4.00	1.25	3.03	45.36
sample 4	7.87	6.39	1.23	2.62	38.56

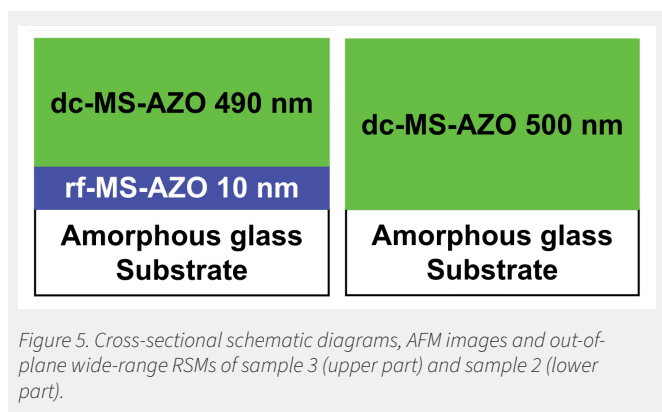


Figure 5. Cross-sectional schematic diagrams, AFM images and out-of-plane wide-range RSMs of sample 3 (upper part) and sample 2 (lower part).

Conclusion

By analyzing the experimental data of the surface morphology and crystallographic orientation distribution of rf- and dc-magnetron-sputtered AZO films of various thicknesses deposited on amorphous glass substrates, we developed a two-step deposition technique using a 10 nm-thick AZO-based critical layer to produce dc-MS-AZO films with a texture that has a preferential c-axis orientation perpendicular to the substrates and a significantly improved surface morphology. The combined results of AFM and XRD provided a comprehensive understanding of key factors governing the crystallographic orientation evolution and surface morphological features in polycrystalline AZO films. Such knowledge can be used to develop the deposition process and conditions to achieve the desired surface morphologies and electrical properties for optoelectronic device applications.

References

- Z. M. Jarzelski, Preparation and physical properties of transparent conducting oxide films, *Phys. Status Solidi*. 71 (1982) 13–41.
- K. L. Chopra, S. Major, D. K. Pandya, Transparent conductors-A status review, *Thin Solid Films* 102 (1983) 1–46.
- P. P. Edwards, A. Porch, M. O. Jones, D. V. Morgan, R. M. Perks, Basic material physics of transparent conducting oxides, *Dalton Trans.* 19 (2004) 2995–3002.
- N. Yamamoto, H. Makino, S. Osone, A. Ujihara, T. Ito, H. Hokari, T. Maruyama, T. Yamamoto, Development of Ga-doped ZnO transparent electrodes for liquid crystal display panels, *Thin Solid Films*, 520 (2012) 4131–4138.
- J. Nomoto, H. Makino, T. Yamamoto, High-Hall-mobility Al-doped ZnO films having textured polycrystalline structure with a well-defined (0001) orientation, *Nanoscale Res. Lett.* (2016) 11:320.
- J. Nomoto, K. Inaba, M. Osada, S. Kobayashi, H. Makino, T. Yamamoto, Highly (0001)-oriented Al-doped ZnO polycrystalline films on amorphous glass substrates, *J. Appl. Phys.* 120 (2016) 125302–1–125302–11.
- J. Nomoto, K. Inaba, S. Kobayashi, H. Makino, T. Yamamoto, Interface layer to tailor the texture and surface morphology of Al-doped ZnO polycrystalline films on glass substrates, *J. Cryst. Growth* 468 (2017) 645–649.
- J. Nomoto, H. Makino, T. Nakajima, T. Tsuchiya, T. Yamamoto, Improvement of the Properties of Direct-Current Magnetron-Sputtered Al-Doped ZnO Polycrystalline Films Containing Retained Ar Atoms Using 10-nm-Thick Buffer Layers, *ACS Omega* 4 (2019) 14526–15536.
- T. Minami, New n-Type Transparent Conducting Oxides, *MRS Bulletin* 25 (2000) 38–44.
- H. Fujiwara, M. Kondo, Effects of carrier concentration on the dielectric function of ZnO:Ga and In₂O₃:Sn studied by spectroscopic ellipsometry: Analysis of free-carrier and band-edge absorption, *Phys. Rev. B* 71 (2005) 075109–1–075109–10.
- T. Yamada, H. Makino, N. Yamamoto, T. Yamamoto, Ingrain and grain boundary scattering effects on electron mobility of transparent conducting polycrystalline Ga-doped ZnO films, *J. Appl. Phys.* 107 (2010) 123534–1–123534–8.
- S. Kobayashi, K. Inaba, X-ray thin-film measurement techniques VIII. Detectors and series summary, *Rigaku J.* 28 (2012) 8–13.
- <https://parksystems.com/products/small-sample-afm/park-nx10/overview>
- H. C. Ward, *Rough Surfaces*, T. R. Thomas Ed., Longman, London cop. (1982).
- B. R. Kumar, T. S. Rao, AFM studies on surface morphology, topography and texture of nanostructured zinc aluminum oxide thin films, *Dig. J. Nanometer. Bios.* 7 (2012) 1881–1889.

PIONEERING FILM DEPOSITION TECHNOLOGY UNCONSTRAINED BY THE FIELD FRAMEWORK

An interview with Professor Tetsuya Yamamoto at Materials Design Center, Kochi University of Technology.

Professor Yamamoto is a Japanese pioneer in zinc oxide research who has successfully fabricated zinc-oxide-based transparent conductive electrodes for use in LCD TV and recently, visualized the alignment of atoms in the process of thin film production, and thereby, innovated a technology that enables atom-scale manufacturing. He developed a reactive plasma deposition device (RPD) that enables fast and low-temperature, low-damage film production jointly with Sumitomo Heavy Industries, Ltd.



Q1: What prompted you to focus on film-forming technology?

My interest in zinc oxide as a material for energy solutions was sparked when I was stationed in the US in 1994. Since then, we have been working to develop functional thin films that are low-temperature, low-energy, and low-damage. Our ultimate goal is to create a product that can be used to address energy issues.

Q2: How did you commercialize film-forming technology?

In 2004, we scaled up production of transparent conductive films using zinc oxide, and in 2012, we developed a new electrode using zinc oxide as a substitute for rare indium, contributing to practical use as a world-standard basic technology. We also developed a technology to generate oxygen negative ions from arc plasma in a plasma deposition device and irradiate them onto metal oxide thin films, controlling surface structure and chemical state at low temperatures and low applied voltage to create functional materials that meet practical needs.

Q3: What specific technology is this?

The uniqueness of this technology lies in the utilization of electrons (e^-) that remain in the plasma deposition apparatus. High electron affinity oxygen gas is injected to film-growth apparatus, adsorbing electrons in a high density to generate oxygen negative ions.

The negatively charged oxygen ions are attracted to the substrate on which the thin film to be treated is deposited. This is because a positive voltage is applied to the substrate with the thin film. This produces oxide thin films exhibiting properties intentionally designed. If the above substrate is only a metal plate substrate, the oxygen-engineering technology will enable to produce a substrate with few defects and in a thermally stable oxide state. Sumitomo Heavy Industries, Ltd. has put this technology into practical use and commercialized it as negatively charged oxygen (O^-) ion generation and irradiation device.

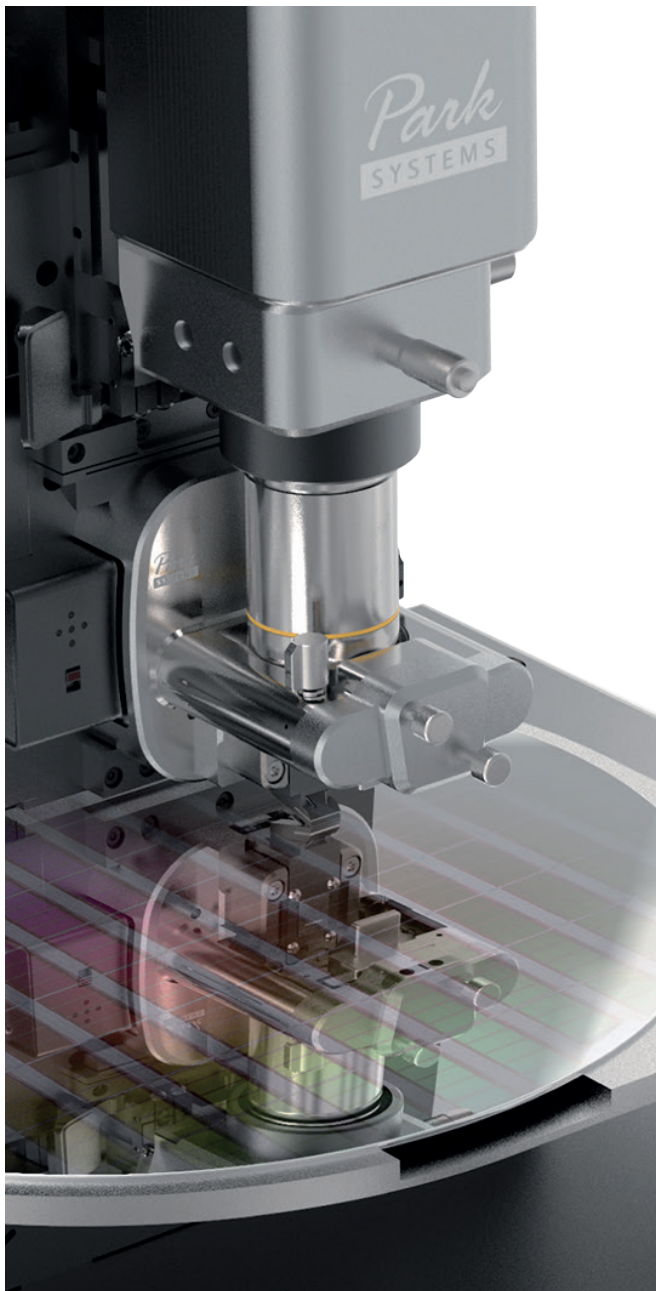
Q4: It was reported that you were able to visualize the arrangement of atoms. How was this possible?

We developed a method of depositing a metal oxide thin film in an amorphous state, where metal atoms and oxygen atoms are randomly arranged at room temperature, on a glass substrate, and gradually heating it from the back side of the substrate. During the heating process, the metal and oxygen atoms move individually, whereas those atoms interact with each other, aligning them from an implicit order state in a short range, as called as amorphous state, into an explicit ordered state in a long range. This forms a lattice system with a space group, as a result. We succeeded in visualizing the dynamic process of changing into a crystalline state in which metal atoms and oxygen atoms are regularly arranged at 180°C. These results are due to joint research and development with Rigaku Corporation.

Q5: What was the key to the successful observation at the atomic scale, and how has that ability enabled the development of a manufacturing process with high reproducibility and good yield?

During the film formation stage, when metal elements and oxygen atoms create strong chemical bonds and the entire film becomes ordered, it becomes difficult to observe dynamic atomic behavior. In other words, in the first stage of the deposition, the key is to create a thin film that is composed of "functional core" consisting of many atoms showing no apparent, however implicit order. By applying appropriate energy to the thin film in the second step, it would become

possible to create a thin film that exhibits intentionally controlled characteristics as functions. Until now, we had to repeat trial and error many times to determine the optimal conditions such as heating temperature and heating time. This visualization technology will provide scientific insight into the atomic order that produces the properties. As a result, the realization of a manufacturing process with high reproducibility and good yield will be embodied. This leads to reduced research and development costs. It can be said that the wisdom of mankind was the catalyst for entering the atomic world. Based on this result and demonstration, we were able to start research on creating low-temperature, low-energy, low-damage functional thin films.



Accurate large Sample AFM solution for **research and failure analysis**



Park **NX20**

As an FA engineer, you're expected to deliver results. There's no room for error in the data provided by your instruments. Park NX20, with its reputation as the world's most accurate large sample AFM, is rated so highly in the semiconductor and hard disk industry for its data accuracy.

parksystems.com/nx20



SURFACE POTENTIAL CHARACTERIZATION OF TWO-DIMENSIONAL MATERIALS THROUGH BACK-GATE VOLTAGE BIASES

Seok-Ju Kang¹, Jong Yun Kim¹, Jaekyung Kim², Oh Hun Gwon¹, and Young-Jun Yu¹

¹ Department of Physics, Chungnam National University, Republic of Korea

² Park Systems Corp., Suwon, Republic of Korea

Introduction

Two-dimensional (2D) materials including semi-metallic graphene, semiconducting transition metal dichalcogenides (TMDs), and insulating hexagonal boron nitride (hBN), have been studied in recent years as electrically or photonically innovative materials. Among various applicable electronic devices, from the specific perspective of memory devices, non-volatile floating gate transistors have been widely researched for high-performance information storage devices.^{1,2} Moreover, the van der Waals (vdW) heterostructures of 2D materials have been further investigated for artificial synaptic emulators for neuromorphic computing systems.^{2,3} In this regard, the typical 2D materials-based floating gate memories are constituted from TMDs, hBN, and graphene as a semiconductor, tunnel barrier, and floating gate, respectively. Furthermore, it is very important to understand the primitive factors, which affect the charge trapping or detrapping behavior in a deep potential well. Therefore, a comprehensive investigation of the 2D material's properties at energy levels is imperative to demonstrate the fast and low-powered flash memories.

For this purpose, the floating gate memory structure was prepared with mechanically exfoliated thin MoS₂, hexagonal boron nitride (hBN), and multilayer graphene (MLG). Afterwards, the work functions of the respective layers depending on the back-gate voltages were examined using a kelvin probe force microscopy (KPFM) apparatus.

Materials and Methods

Transfer process for 2D materials

Flakes of each 2D material (MoS₂, hBN, and MLG) were exfoliated onto a rectangular piece of cured polydimethylsiloxane (PDMS) by mechanical exfoliation with the standard scotch tape method⁴. Subsequently, the exfoliated 2D materials were transferred slowly onto the SiO₂/p⁺Si substrate in the order of MoS₂/hBN/MLG stacking. During the transfer process, the 2D flakes on PDMS were precisely aligned with the intended position on the target substrate by a micro-manipulator and were then brought into contact.

KPFM measurement with gate bias

KPFM measurements were obtained using a commercial atomic force microscopy (AFM) system (Park NX10, Park Systems Corp.) at room temperature in air. An Au-coated cantilever with a Cr sublayer on an n-type silicon material (Mikromash corp., spring constant: 1 N/m, resonance frequency: 90 kHz) was used as the conductive tip. During the observation of the surface potential data, an AC voltage amplitude of ~2 V and a frequency of 17 kHz were applied to a conductive probe. The surface potential was obtained by applying a feedback DC voltage (V_{DC}) with a lock-in amplifier to cancel the electrostatic force between the Au-coated tip and the sample generated by the AC voltage (V_{AC}) applied to the tip.^{5,6} To investigate the effect of the back-gate bias (V_{BG}) during KPFM analysis, changes in surface potential were observed while maintaining a constant V_{BG} bias by sequentially applying a V_{BG} of 0 V or 40 V. The morphology and surface potential data were later analyzed using Park Systems analysis software to retrieve numerical information from the measured mapping images.

Results and Discussion

To fabricate multi-stacked 2D heterostructures, the MLG, hBN, and MoS₂ were transferred sequentially to a SiO₂/p⁺Si substrate, as shown in Fig. 1a. The transferred MLG, hBN, and MoS₂ are adopted to fulfill the roles of semi-metal, wide bandgap insulator, and semiconductor, respectively. The multi-stacked heterolayers were characterized through the KPFM setup with applied V_{BG} to examine the surface potential variances of each 2D layer depending on the back-gated voltages, as presented in Fig. 1b. In this system, the Fermi levels or work-functions could be changed under the back-gate bias.

The multi-stacked heterostructure was constructed successfully as observed by optical microscopy and presented in Fig. 2a. The surfaces of the layers remained largely uncontaminated during the transfer process, such that the topographic and electrical information were not affected.

From the height profile of a line-scan indicated in the AFM morphology image, the thicknesses of MoS₂, hBN, and MLG could be calculated to approximate values of 6.9, 60.5, and 12.0 nm, respectively. The overall stacking structure with each thickness value for the three layers is presented in Fig. 2d.

To verify the different behavior of MoS₂-based floating gate memory devices, the surface potentials and the work-functions of MoS₂, hBN, and MLG were measured using a KPFM system where V_{BG} was applied as shown in Figs. 3a, b and 3d, e, respectively.

The KPFM measurements yielded the

contact potential difference (V_{CPD}) between the Au-coated AFM tip and the sample, and the following relationship was obtained.

$$eV_{CPD} = WF_{tip} - WF_{sample} \Rightarrow WF_{sample} = WF_{tip} - eV_{CPD} \quad (1)$$

where WF_{sample} and WF_{tip} are the work functions of the sample and tip, respectively, and e is the electronic charge.

Since the vdW heterostructure is floating on a SiO_2 substrate, the contact potential and the work function of MLG were used as standard points. As a result, the contact potential or work function differences between the various multi-stacking layers and MLG could be described as the equations below.

For the hBN/MLG stacking layers,

$$\Delta V_{CPD(hBN/MLG)} = V_{CPD(hBN/MLG)} - V_{CPD(MLG)} \equiv \Delta V_{H-G} \quad (2)$$

$$\Delta WF_{(hBN)/(MLG)} = WF_{(hBN)/(MLG)} - WF_{(MLG)} \equiv \Delta WF_{(H-G)} \quad (3)$$

For the MoS_2 /hBN/MLG stacking layers,

$$\Delta V_{CPD(MoS_2/hBN/MLG)} = V_{CPD(MoS_2/hBN/MLG)} - V_{CPD(MLG)} \equiv \Delta V_{(M-G)} \quad (4)$$

$$\Delta WF_{(MoS_2/hBN/MLG)} = WF_{(MoS_2/hBN/MLG)} - WF_{(MLG)} \equiv \Delta WF_{(M-G)} \quad (5)$$

The work-function difference (ΔWF_{H-G} or ΔWF_{M-G}) was calculated through equation (3) for hBN or equation (5) for MoS_2 . As seen in Figs. 3c, f, while applying a V_{BG} bias of 40 V, the Fermi energy levels of each stacked 2D material (MoS_2 , and hBN) were shifted higher from the initial positions ($V_{BG} = 0$ V) with respect to the work-function level of MLG.

In the case of ' $V_{BG} = 0$ V', the work-function differences for the two surfaces of hBN/MLG (ΔWF_{H-G}) and MoS_2 /hBN/MLG (ΔWF_{M-G}) layers are ca. -171.9 meV and ca. -265.8 meV, respectively. Thus, the Fermi levels are positioned lower than the MLG work function level. However, in the case of ' $V_{BG} = 40$ V', the work-function differences for the two surfaces of hBN/MLG (ΔWF_{H-G}) and MoS_2 /hBN/MLG (ΔWF_{M-G}) layers are ca. 89.0 meV and ca. 125.2 meV, respectively. Hence, the Fermi levels are positioned higher than the MLG work function level.

Due to the different work-function level behaviors depending on the V_{BG} bias, the MLG layer can be efficiently charged with electrons or holes by tunneling.

To summarize the results, under the V_{BG} condition of 0 V, electrons in the MLG layer could migrate more easily to the MoS_2 layer by overcoming the barrier of the hBN layer. Contrary to this, for the V_{BG} condition of 40 V, the MLG layer would be convenient to obtain electrons from the MoS_2 layer with a reduced energy barrier between MoS_2 and hBN layers.



The most accurate and easiest to use Atomic Force Microscope Park NX10

Park
SYSTEMS

Please visit parksystems.com/nx10 to learn more about Park NX10

Conclusion

For the study of the charge transfer behavior through the hBN insulating layer, the back-gated KPFM mode was utilized as a method to investigate the surface potential properties of 2D materials when back-gate voltages of 0 and 40 V were applied. Through the method of the back-gated KPFM, the cause of the charging and discharging behavior of the graphene layers embedded in the structure of a MoS₂/hBN/MLG on SiO₂/p⁺⁺Si substrate was scrutinized.

Ultimately, the back-gated KPFM method can be widely employed to characterize the device operation mechanisms of non-volatile floating gate memories, memtransistors, and various other electrically functional devices.

References

- [1] Bertolazzi, S.; Bonnavalli, P.; Roche, S.; San, T.; Choi, S. Y.; Colombo, L.; Bonaccorso, F.; Samori, P., Nonvolatile Memories Based on Graphene and Related 2D Materials. *Adv Mater* 2019, 31 (10), e1806663.
- [2] Seo, S.; Lee, J. J.; Lee, H. J.; Lee, H. W.; Oh, S.; Lee, J. J.; Heo, K.; Park, J. H., Recent Progress in Artificial Synapses Based on Two-Dimensional van der Waals Materials for Brain-Inspired Computing. *ACS Appl Electron Ma* 2020, 2 (2), 371-388.
- [3] Yi, S. G.; Park, M. U.; Kim, S. H.; Lee, C. J.; Kwon, J.; Lee, G. H.; Yoo, K. H., Artificial Synaptic Emulators Based on MoS₂ Flash Memory Devices with Double Floating Gates. *ACS Appl Mater Interfaces* 2018, 10 (37), 31480-31487.
- [4] Huang, Y.; Sutter, E.; Shi, N. N.; Zheng, J.; Yang, T.; Englund, D.; Gao, H. J.; Sutter, P., Reliable Exfoliation of Large-Area High-Quality Flakes of Graphene and Other Two-Dimensional Materials. *ACS Nano* 2015, 9 (11), 10612-20.
- [5] Yu, Y. J.; Choe, J. H.; Kim, J. Y.; Gwon, O. H.; Choi, H. K.; Choi, J. S.; Kim, J. H.; Kim, J. S.; Kim, J. T.; Shin, J. H.; Choi, Y. K., Gate-tuned conductance of graphene-ribbon junctions with nanoscale width variations. *Nanoscale* 2019, 11 (11), 4735-4742.
- [6] Yu, Y. J.; Zhao, Y.; Ryu, S.; Brus, L. E.; Kim, K. S.; Kim, P., Tuning the graphene work function by electric field effect. *Nano Lett* 2009, 9 (10), 3430-4.

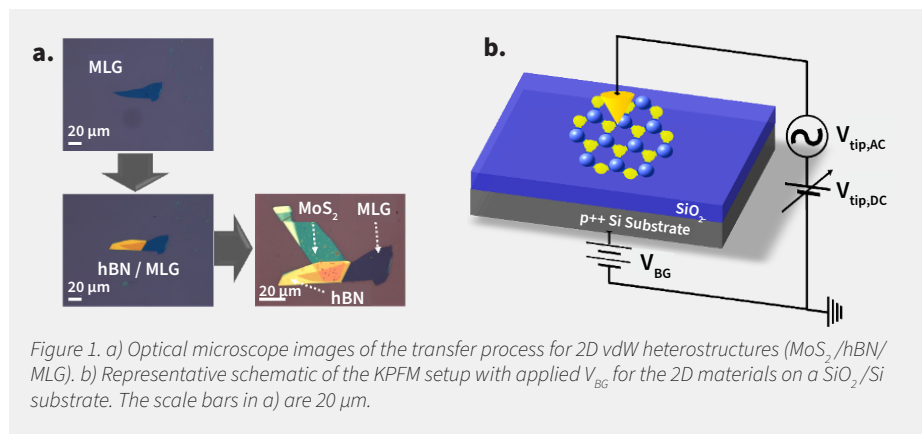


Figure 1. a) Optical microscope images of the transfer process for 2D vdW heterostructures (MoS₂/hBN/MLG). b) Representative schematic of the KPFM setup with applied V_{BG} for the 2D materials on a SiO₂/Si substrate. The scale bars in a) are 20 μm.

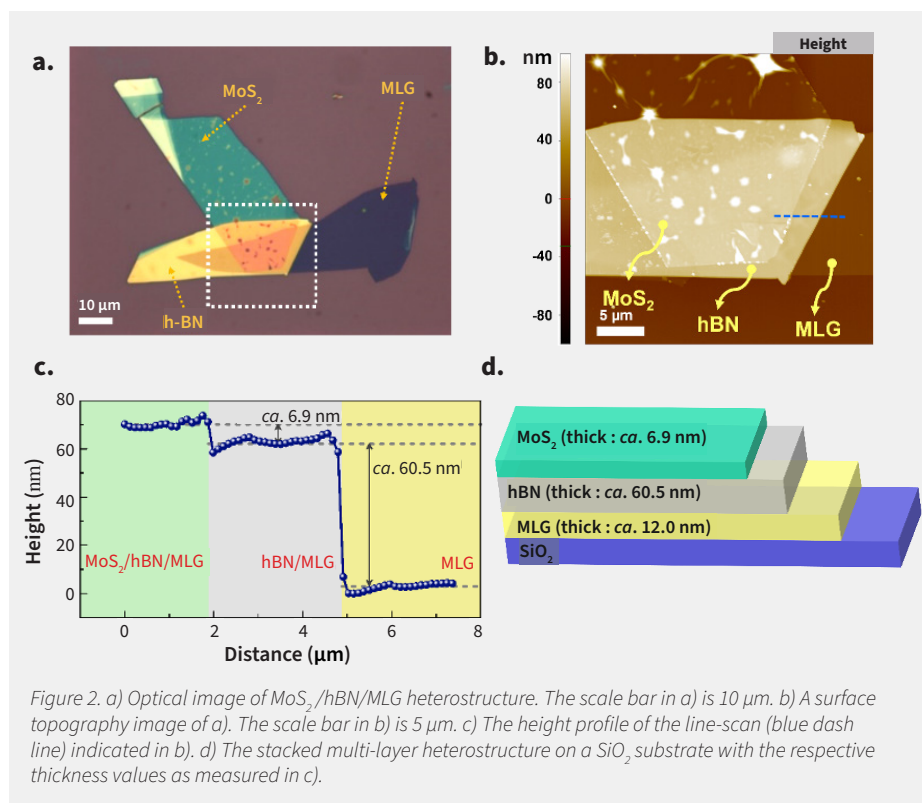


Figure 2. a) Optical image of MoS₂/hBN/MLG heterostructure. The scale bar in a) is 10 μm. b) A surface topography image of a). The scale bar in b) is 5 μm. c) The height profile of the line-scan (blue dash line) indicated in b). d) The stacked multi-layer heterostructure on a SiO₂ substrate with the respective thickness values as measured in c).

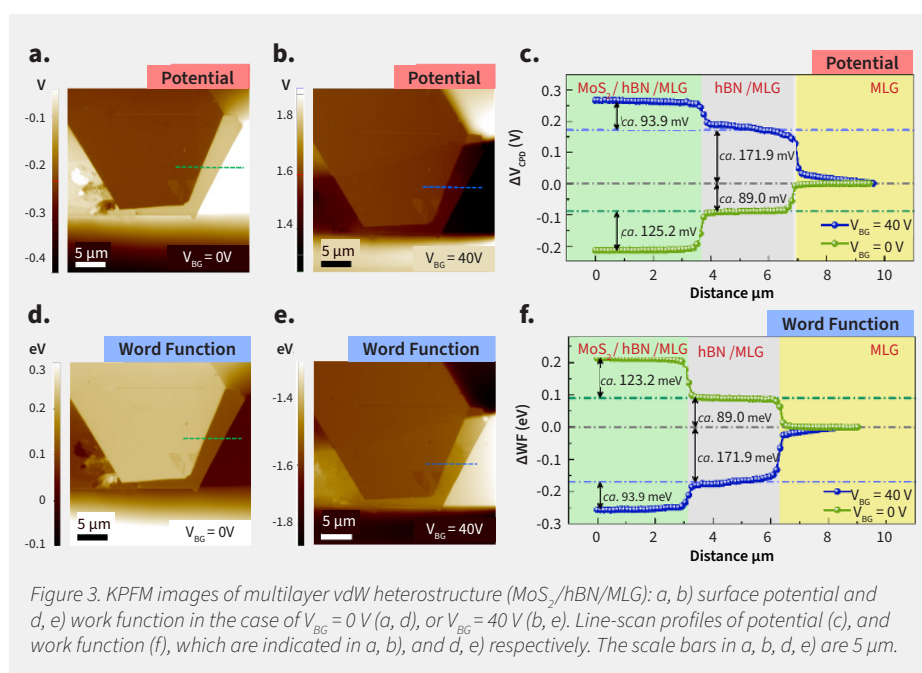


Figure 3. KPFM images of multilayer vdW heterostructure (MoS₂/hBN/MLG): a, b) surface potential and d, e) work function in the case of V_{BG} = 0 V (a, d), or V_{BG} = 40 V (b, e). Line-scan profiles of potential (c), and work function (f), which are indicated in a, b), and d, e) respectively. The scale bars in a, b, d, e) are 5 μm.

MAPPING THE REGISTRY AND FUNCTIONAL PROPERTIES OF LAYERED MATERIALS HETEROSTRUCTURES USING CONDUCTIVE ATOMIC FORCE MICROSCOPY

J. Kerfoot, V. V. Korolkov. Park Systems UK Ltd, Nottingham, UK

Overview

Manipulating the registry of layers within layered materials heterostructures leads to changes in their functional properties both locally [1,2] and at scales relevant to devices [2,3]. This motivates interest in atomic force microscopy (AFM) as a tool capable of resolving both inter-layer registry and a host of concomitant functional properties at nanometre length scales. Here, we showcase conductive AFM (C-AFM) as a technique capable of determining the registry of layers and extracting functional properties via spectroscopic measurements over individual features.

When two rigid layers with a fixed spatial periodicity are overlaid, a moiré pattern may be observed. The symmetry of such features is dependent upon the symmetry of the overlaid layers and

the periodicity is dependent upon the mismatch in period of the two features and the angle between them. Moiré patterns can be observed in many situations including in overlaid fabrics and installations such as bridges but most recently moiré patterns have received significant interest for their influence over the functional properties of layered materials heterostructures, namely the field of twistrionics [3,4]. One prominent example of where moiré patterns have been explored in layered materials heterostructures is the case of single layer graphene (SLG) on hexagonal boron nitride (hBN). Using hBN as a substrate [5] and encapsulant [6] of SLG enables the fabrication of devices in which the effects of contaminant induced doping is suppressed, yielding state-of-the-art performance characteristics such as mobility. For SLG on hBN, a hexagonal moiré period is seen owing

to the hexagonal symmetry and small, ~ 2%, spatial mismatch between hBN and SLG (see figure 1 b-d). Samples were first fabricated by exfoliating both hBN (HQ graphene) and graphene on thermally grown SiO₂ before flakes were sequentially picked up and transferred onto pre-deposited contacts using polymeric stamps. After removing polymer residue through solvent immersion and then mechanically by performing contact mode AFM over the area of interest, samples were measured using C-AFM on the Park FX40 automatic AFM with ElectriMulti75-G probes (see fig 1 e and f).

Conductive AFM utilises the same setup as contact mode AFM (with associated mechanical setpoint: SP_{Mech}) to maintain the tip in contact with the surface under constant mechanical load via a feedback loop which also allows the

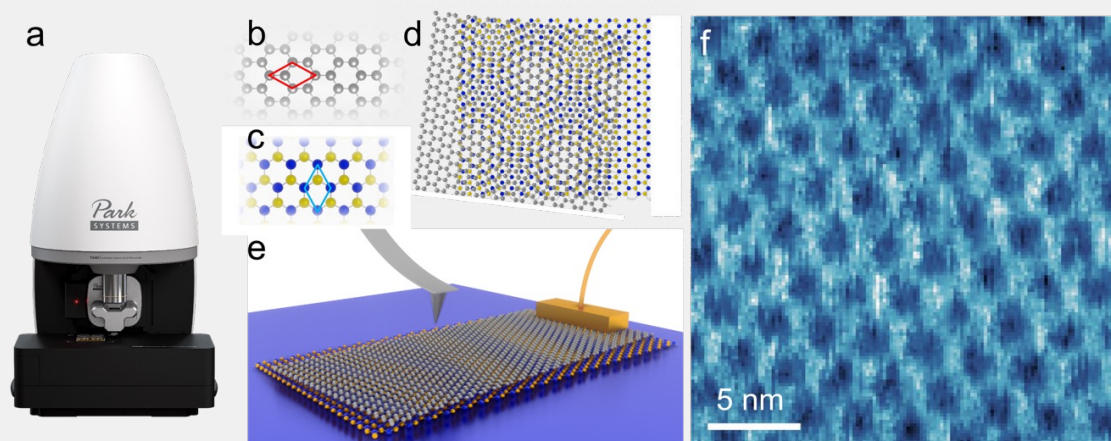


Figure 1. Using the Park Systems FX40 automatic AFM (a), C-AFM measurements were performed in contact mode to map the morphology of moiré patterns. A heterostructure of single layer graphene (SLG) (b) on hexagonal boron nitride (hBN) (c) was produced by stacking mechanically exfoliated flakes. The similar lattice constants of hBN and SLG give rise to a moiré pattern, as depicted for a twisted heterostructure (d). With an electrode applied to the substrate and the tip-sample interaction controlled via contact mode (e), current maps acquired under constant voltage may be measured (f) which reveal a hexagonal moiré pattern due to the spatially modulated stacking registry of hBN and SLG.

topography to be extracted. By applying an electrical contact to the sample and using a conductive probe, the current may be measured at the tip sample junction and mapped spatially with sub-nanometre resolution. Such current maps of SLG/hBN (see figure 1f and 2a) reveal a hexagonal moiré pattern with areas of higher current observed for the network of domain boundaries compared to the central regions where the lattices stack in a more parallel fashion [7]. When using C-AFM, structures are immediately observed in the in the current channel without significant modification of setpoints. The contrast of such features in AFM images may be improved by optimising SP_{Mech} , the voltage applied between the tip and sample (V_{TS}), increasing the scan rate to suppress thermal drift and changing the state of the tip by applying short and controlled pulses of higher voltage. Upon optimisation of the aforementioned acquisition parameters, current maps showing nanometre scale corrugations (see figure 2a and 2b) may be acquired, with extracted line profiles showing remarkable conformity.

In general, for layered materials heterostructures, the intra-layer forces arising from bonding within layers are stronger than inter-layer forces arising from van der Waals interactions. For this reason, layered materials heterostructures typically exhibit moiré patterns as the stronger intra-layer interactions yield comparatively rigid layers which are not disrupted even when small relaxations may lead to favourable inter-layer adhesion energies [8]. In some special instances however, layered materials heterostructures may be formed between layers of the same or similar lattice constant and marginal twist angle (typically $< 2^\circ$) such that inter-layer interactions are sufficient to induce changes in the intra-layer structure, known as atomic reconstruction and demonstrated for the first time in marginally twisted bilayer MoS_2 by Weston et al [9,10].

We fabricated such samples using the so called ‘tear and stack’ method [11], by first exfoliating 1L- MoS_2 (SPI supplies) on polydimethylsiloxane (PDMS) using scotch tape. The flake was then brought partially into contact with a freshly cleaved highly oriented pyrolytic graphite (HOPG) surface and retracted, such that the flake broke, with part left on the

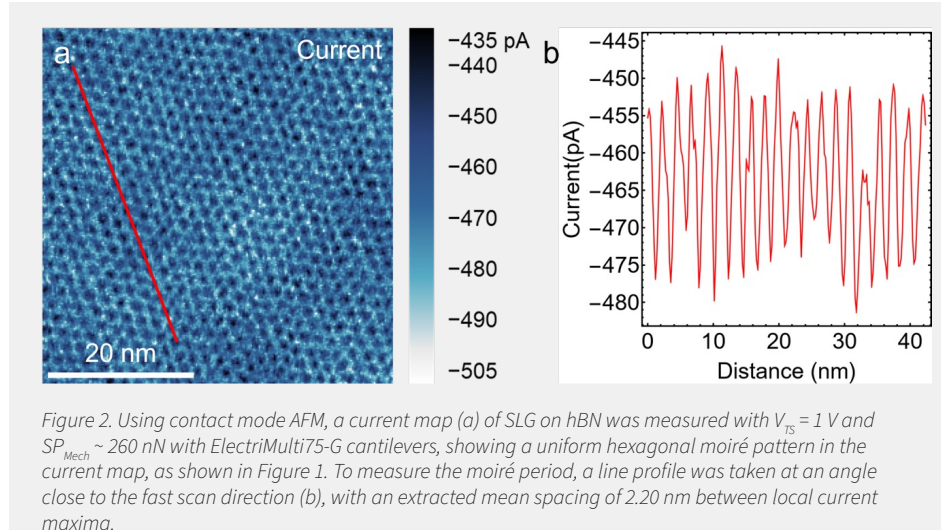


Figure 2. Using contact mode AFM, a current map (a) of SLG on hBN was measured with $V_{TS} = 1$ V and $SP_{Mech} \sim 260$ nN with ElectriMulti75-G cantilevers, showing a uniform hexagonal moiré pattern in the current map, as shown in Figure 1. To measure the moiré period, a line profile was taken at an angle close to the fast scan direction (b), with an extracted mean spacing of 2.20 nm between local current maxima.

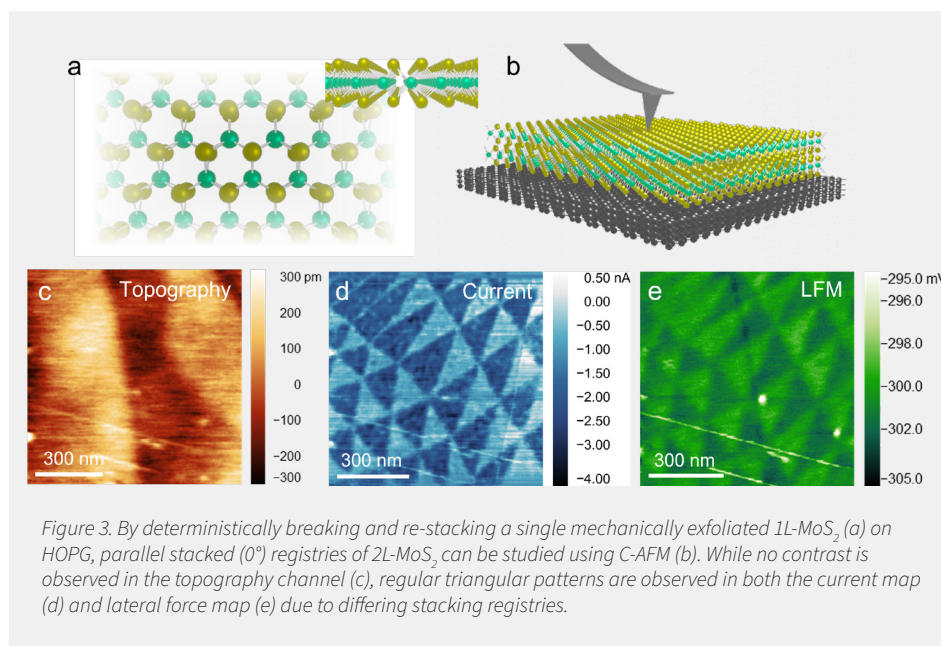


Figure 3. By deterministically breaking and re-stacking a single mechanically exfoliated 1L- MoS_2 (a) on HOPG, parallel stacked (0°) registries of 2L- MoS_2 can be studied using C-AFM (b). While no contrast is observed in the topography channel (c), regular triangular patterns are observed in both the current map (d) and lateral force map (e) due to differing stacking registries.

HOPG before the remaining 1L- MoS_2 on PDMS was aligned to the first flake and stacked on top. By breaking and restacking the same flake, the twist angle between two layers can be controlled deterministically (0° was used here). Before measuring using C-AFM, samples were annealed to $150^\circ C$ for 5 minutes in air before cooling to room temperature and scanned using contact mode AFM to promote the removal of contamination from the top MoS_2 surface and buried interfaces.

The cleaned 2L- MoS_2 (0°) on HOPG was measured using C-AFM (see figure 3b) with $V_{TS} = 0.5$ V and $V_{SPMech} \sim 65$ nN, with regular triangular domains observed in both the current and lateral force channels (see figure 3 d and e) but not in topography (see figure 3c). Contrast between current of AB/BA domains

with stacking registries (offset by half a unit cell) was in good agreement with observations in the literature [9,12]. In addition to the current map, contrast was measured in the lateral force image (the deflection of the cantilever parallel to the scan direction and perpendicular to the cantilever) which implies differences in the mechanical interaction between the tip and 2L- MoS_2 across different domains.

Comparing different areas of the same 2L- MoS_2 (0°) on HOPG sample, areas of comparatively regular triangular domain morphology (see figure 3d) are observed in addition to more distorted structures (see figure 4a), which we attribute to uneven distributions of strain induced mechanically during sample fabrication. In addition to measuring the morphology of such domains, C-AFM allows the current-voltage characteristics of the

junction between the tip and sample to be measured from isolated locations. By performing arrays of point current-voltage measurements across a pre-mapped region, current voltage maps from specific domains may be measured, as shown in figure 4b, to isolate the properties of specific registries and gain insights into how local variations affect the performance of completed devices.

Conclusions

Stacking layered materials to form heterostructures may induce structural features such as moiré patterns and atomic reconstruction, which influences functional properties locally and at device scales. Here, we have shown that C-AFM enables such features in electrically conductive samples to be measured with nanometre scale resolution and highly relevant functional

properties measured via mapping and spectroscopy. The advantage of C-AFM is that it provides information on the electrical properties of materials at nanometre length scales which are complementary to device characterisation techniques. Such insights are valuable both in exploring the fundamental properties of twisted layered materials heterostructures and in the optimisation of devices such as transistors, memristors, photodetectors and light emitting diodes.

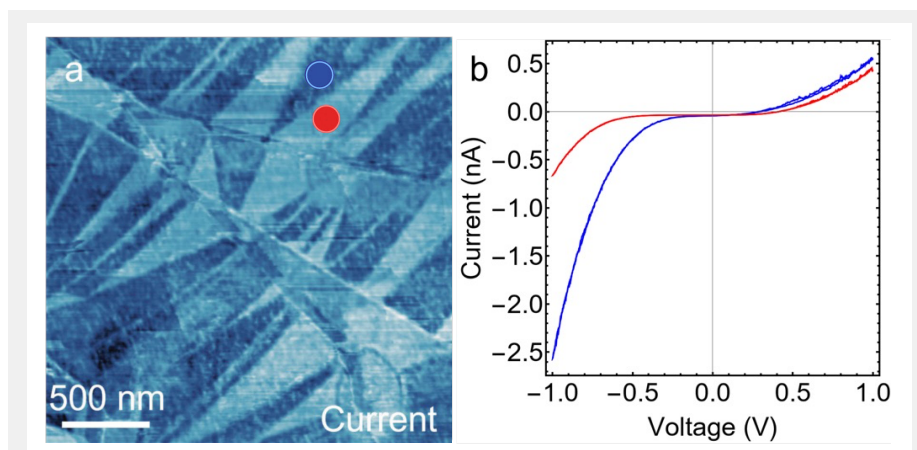
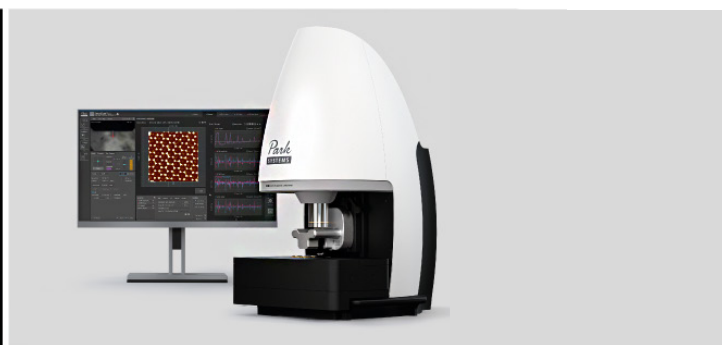


Figure 4. For the same parallel stacked 2L-MoS₂/HOPG sample shown in figure 3, a larger area current map was measured, revealing less regular distorted domains (a). By positioning the probe over specific domains, current-voltage curves may be measured (b), revealing differing characteristics over regions of high and low current contrast.

References

- [1] E. Li et al. Nat Commun. 12, 5601 (2021).
- [2] X. Wang et al. Nat. Nanotechnol. 17, 367 (2022).
- [3] R. Ribeiro-Palau et al. Science 361, 6403, 690 (2018).
- [4] Y. Cao et al. Nature 556, 80 (2018).
- [5] C. Dean et al. Nat. Nanotechnol. 5, 722 (2010).
- [6] D. G. Purdie et al. Nat. Commun. 9, 5387 (2018).
- [7] C. Woods et al. Nature Phys. 10, 451 (2014).
- [8] V. V. Enaldiev et al. PRL 124, 206101 (2020).
- [9] A. Weston et al. Nat. Nanotechnol. 15, 592 (2020).
- [10] A. Weston et al. Nat. Nanotechnol. 17, 390 (2022).
- [11] K. Kim et al. Nano Lett. 16, 3, 1989 (2016).
- [12] M. R. Rosenberger et al. ACS Nano 14, 4, 4550 (2020).



Park FX40

**A Groundbreaking New Class of AFM
The Autonomous Atomic Force Microscope**

Built-in Intelligence - It does all your set up and scanning so that you can focus on your research.



SCAN ME!
Watch the video

parksystems.com/fx40

**Park
SYSTEMS**

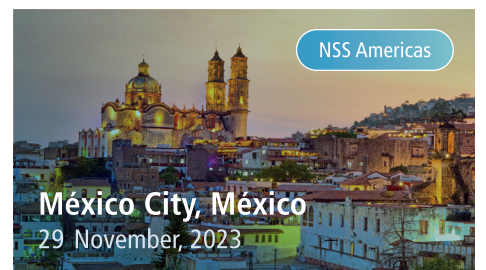


2023 NANOscientific Symposium Scanning Probe Microscopy (SPM)

REGISTER NOW!

Join us for a truly international symposium on scanning probe microscopy! NANOscientific event will feature speakers from across the world, presenting groundbreaking research and discussing the latest advancements and techniques in SPM. Don't miss this opportunity to connect with the worldwide community of SPM researchers and expand your knowledge of this exciting field.

NANOscientific symposium brings together experts from around the globe to explore the science, engineering, and applications of nanotechnology. Featuring keynote addresses and virtual networking opportunities, attendees can form connections and propel their research, innovation, and businesses forward.



Sponsored By

NANOscientific

Park
SYSTEMS

NWA
NANOTECHNOLOGY
WORLD ASSOCIATION

PARK SYSTEMS INTRODUCES PARK NX-IR R300 AND PARK NANOSTANDARD

Park Systems, a leading manufacturer of atomic force microscopy (AFM) and nano metrology systems, has launched two new products to its portfolio of nanoscale metrology solutions for the semiconductor industry. The Park NX-IR R300 is a nanoscale infrared spectroscopy (IR) system that provides chemical property information, mechanical and topographical data for semiconductor research, failure analysis, and defect characterization at an unprecedented high nano resolution. The Park NANOSTandard™ product line provides calibration standard samples for AFM and SEM measurements, allowing users to accurately measure and analyze their samples.

The Park NX-IR R300 combines infrared spectroscopy and AFM into one system that can handle up to 300 mm semiconductor wafers. It uses the most advanced IR spectroscopy of photo-induced force microscopy (PiFM) onto the industry-leading Park NX20 300 mm AFM platform. PiFM spectroscopy provides chemical identification under 10 nm spatial resolution, enabling damage-free spectroscopy probing, highest resolution, and accuracy throughout scans. The Park PiFM provides the user with spectroscopy information at varying depths, offering invaluable insight into sample composition. The Park NX-IR R300 is an essential tool for industrial customers who need to analyze the

chemical composition of their materials at the highest level of accuracy.



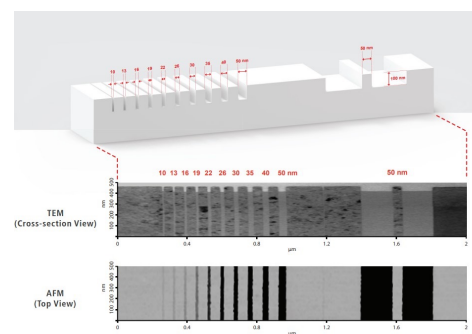
Park NX-IR 300

The Park NANOSTandard product line provides reliable and accurate calibration of AFM and SEM systems, allowing users to accurately measure and analyze their samples. The product line includes AFM Tip Characterizer (AFMTC) and High Magnification Calibration (HMC). The AFMTC is a calibration sample designed to evaluate the radius and half-cone angle of an AFM tip. It is nano-patterned with line widths ranging from 10 nm to 50 nm and is traceable to the Korean Research Institute of Standards and Science (KRISS) for ISO 17034:2016. The HMC standard sample is made of polycrystalline silicon and has five certified values for line widths ranging from 20 nm to 80 nm and five certified values for pitch values ranging from 100 nm to 900 nm. The HMC standard sample is traceable to the KRISS for ISO 17034:2016.

"The Park NX-IR R300 and Park NANOSTandard product line are major advancements in our portfolio of nanoscale metrology solutions," said Dr. Sang-il Park, CEO of Park Systems. "They represent our continued expansion into new areas of innovation for nanometric microscopy tools for engineers and scientists in industry and research labs. We are confident that the Park NX-IR R300 and Park NANOSTandard will become essential tools for industrial customers who need to ensure the accuracy of their measurements and increase the quality of their products."

The Park NANOSTandard products are manufactured in collaboration with Kims Reference Corp., a leading manufacturer of advanced reference materials for nano-measurement and surface analysis. "We are proud to be collaborating with Kims Reference Corp. to bring this innovative

product line to market," said VP of Product Marketing, Richard Lee. "The Park NANOSTandard product line will help our customers ensure the accuracy of their measurements and increase the quality of their products."



Park NANOSTandard AFM Tip Characterizer



PARK SYSTEMS CORPORATION ACQUIRES ACCURION GMBH

Park Systems has made a strategic move to expand its business portfolio by acquiring Accurion GmbH. The Germany-based company specializes in developing and manufacturing imaging spectroscopic ellipsometers (ISE) and active vibration isolations (AVI).

During the merger and acquisition ceremony that was held in Goettingen, Germany, Dr. Sang-il Park, the CEO of Park Systems, expressed his excitement about the new venture. "Today is a historical moment in this company and in my life because it is a start of a new chapter. We are starting the 3rd venture, which goes beyond the AFM. We are planning to develop new ISE solutions for industrial applications, improve the AVI performance for AFM needs, and to use the power of Park Systems's brand to globally promote and distribute Accurion products," he said while cutting the red ribbon at the new Park GMBH's facility.

The new company name for Accurion was announced: Park Systems GmbH, Accurion Division. The CEO of the new Park Systems GmbH, Stephan Ferneding, expressed his confidence in the partnership. "I'm very convinced that we have chosen a very good partner with many synergies that are not only good for Park's business, but also for Accurion's in these turbulent times," he added.

The merger of Accurion with Park Systems brings a new era for Park's metrology products that rise above the AFM technology. Dr. Park revealed, "By combining the Imaging Spectroscopy and Ellipsometry module to Park Systems platform, we can easily create new ISE solutions for the semiconductor industry. All of that will expand our business portfolio beyond AFM, which is a significant step to fuel our company's growth."

Since its foundation in 1997, Park Systems has established over 14



Sang-il Park (CEO of Park Systems) and Stephan Ferneding (the CEO of Accurion) open the curtain together marking the merger of Accurion to Park Systems

facilities worldwide and nanoscience centers equipped with a full range of research and industrial AFM tools. Alongside academic and key industrial partners, Park Systems has continuously developed and established new innovative nanometrology standards for the future.

Kristof Paredis, the R&D Manager from imec, the world-leading R&D and innovation hub in nanoelectronics and digital technologies and a longtime joint development partner of Park Systems, commented on the growth of Park Systems in recent years, stating that it has been helpful for joint development efforts with Park.

The ribbon cutting of Park Systems M&A of Accurion marked the beginning of the next phase of expansion of Park Systems' business to execute its mission of enabling nanoscale advances.

Accurion, with its 30 years of valuable experience in enabling technological and scientific progress for customers worldwide, provides high-end and reliable state-of-the-art technology in two product lines: Imaging Ellipsometry and Active Vibration Isolation. In 2009, Halcyonics GmbH, a specialist for active vibration isolation solutions, and Nanofilm Technology GmbH, an expert for surface analyzing tools, merged into Accurion GmbH.

The strategic move by Park Systems to expand its business portfolio is a significant step towards the company's growth and to fuel further advancements in nanotechnology. This merger and acquisition with Accurion opens up a new world of possibilities for Park Systems beyond AFM technology. It will be exciting to see the developments that arise from this partnership in the near future.

Active Vibration Isolation System

The Ultimate Stability and Accuracy Solution for Your Scientific Research



Accurion i4

Introducing the Accurion i4, a cutting-edge active vibration isolation system designed for high-resolution measurement equipment. Equipped with active compensation in all six degrees of freedom, the Accurion i4 is capable of effectively isolating vibrations and disturbances originating from buildings. The system's exceptional performance is highlighted by its ability to commence vibration isolation at a mere 0.6 Hz, ultimately reaching peak isolation of 99.0% at 10 Hz with an impressive -40 dB of noise attenuation. The Accurion i4 boasts three distinct versions that provide unparalleled versatility, all of which are user-friendly and easily operated with low-profile designs.

- Unmatched stability and precision with dynamic vibration isolation in six degrees of freedom.
- Fast settling time of 0.3 seconds or under with auto load adjustment and transport lock.
- Advanced active vibration isolation system with instant counterforce for maximum precision.
- Versatile vibration isolation.

Don't let vibrations and disturbances disrupt your research. Visit www.parksystems.com/i4 for more information.

Park
SYSTEMS
inquiry@parksystems.com

One Nanostep for Microscopy One Giant Leap for Science



Park FX40

A New Class of Atomic Force Microscope

Effortlessly, get the sharpest, clearest, highest resolution images and measurements one sample after another on various applications. Boost your progress and scientific discoveries through unprecedented speed and accuracy – as the Park FX40 autonomously images and acquires data powered by its artificial intelligence, robotics and machine learning capability.



Watch the video